Dannhaus, N., Wittmann, H., Krám, P., Christl, M., von Blanckenburg, F. (2018): Catchment-wide weathering and erosion rates of mafic, ultramafic, and granitic rock from cosmogenic meteoric 10 Be/ 9 Be ratios. - *Geochimica et Cosmochimica Acta*, *222*, pp. 618—641.

DOI: http://doi.org/10.1016/j.gca.2017.11.005

Catchment-wide weathering and erosion rates of mafic, ultramafic, and granitic rock from cosmogenic meteoric $^{10}Be/^{9}Be$ ratios

N. Dannhaus[a], H. Wittmann[a,*], P. Krám[b], M. Christl[c], F. von Blanckenburg[a,d]

*Corresponding author. Email: Wittmann @gfz-potsdam.de
[a]GFZ German Research Centre for Geosciences, Telegrafenberg, 14473 Potsdam, Germany
[b]Czech Geological Survey, Klárov 3, 11821 Prague1, Czech Republic
[c]Lab for Ion Beam Physics, ETH Zurich, HPK H25, 8093 Zurich, Switzerland
[d]Freie Universität Berlin, Institute for Geological Sciences, Malteserstr. 74-100, 12249 Berlin, Germany

Abstract

Quantifying rates of weathering and erosion of mafic rocks is essential for estimating changes to the oceans alkalinity budget that plays a significant role in regulating atmospheric CO_2 levels. In this study, we present catchment-wide rates of weathering, erosion, and denudation measured with cosmogenic nuclides in mafic and ultramafic rock. We use the ratio of the meteoric cosmogenic nuclide ^{10}Be, deposited from the atmosphere onto the weathering zone, to stable ^{9}Be, a trace metal released by silicate weathering. We tested this approach in stream sediment and water from three upland forested catchments in the north-west Czech Republic. The catchments are underlain by felsic (granite), mafic (amphibolite) and ultramafic (serpentinite) lithologies. Due to acid rain deposition in the 20th century, the waters in the granite catchment exhibit acidic pH, whereas waters in the mafic catchments exhibit neutral to alkaline pH values due to their acid buffering capability. The atmospheric depositional ^{10}Be flux is estimated to be balanced with the streams' dissolved and particulate meteoric ^{10}Be export flux to within a factor of two. We suggest a correlation method to derive bedrock Be concentrations, required as an input parameter, which are highly heterogeneous in these small catchments.

Derived Earth surface metrics comprise 1) Denudation rates calculated from the $^{10}Be/^{9}Be$ ratio of the "reactive" Be (meaning sorbed to mineral surfaces) range between 110 to 185 t km^{-2} y^{-1} (40 to 70 mm ky^{-1}). These rates are similar to denudation rates we obtained from *in situ*-cosmogenic ^{10}Be in quartz minerals present in the bedrock or in quartz veins in the felsic and the mafic catchment. 2) The degree of weathering, calculated from the fraction of ^{9}Be released from primary minerals as a new proxy, is about 40 to 50% in the mafic catchments, and 10% in the granitic catchments. Lastly, 3) erosion rates were calculated from ^{10}Be concentrations in river sediment and corrected for sorting and dissolved loss. These amount to 50% of denudation rates from $^{10}Be/^{9}Be$ in the mafic and ultramafic catchments, the remainder being mass loss in the dissolved form by weathering. In contrast, erosion comprises most of the mass loss in the granitic catchment.

These first results are encouraging, given that we find overall good agreement between *in situ* and meteoric cosmogenic methods, that our denudation rates are in the range of those published for middle European river catchments, and that degrees of weathering are as expected for these diverse lithologies. This method allows quantifying rates of erosion and weathering in mafic rock over the time scale of weathering that are, unlike

in situ cosmogenic ^{10}Be, independent from the presence of quartz. ^{10}Be/^{9}Be therefore offers to quantify Earth surface processes in a wide range of landscapes underlain by mafic rock – rates that are of high importance for exploring climate-weathering feedbacks but that have been inaccessible to date.

1. Introduction

About 30% of the global alkalinity flux into the oceans is derived from weathering of mafic rock (Dessert et al., 2003; Gaillardet et al., 1999; Schopka et al., 2011). Because of their high proportion of Mg and Ca, weathering of mafic rocks exerts a sensitive control for regulating atmospheric CO_2 levels (e.g. Berner (1995); Goodwin et al. (2009); Goudie and Viles (2012); Ibarra et al. (2016)). As such, quantitatively constraining the erosion and weathering rates of areas underlain by mafic and ultramafic rocks is paramount. However, methods based on river load gauging do not integrate over weathering time scales, roughly defined as the interval required to form and erode a layer of soil, typically ~10^3 to 10^4 yrs. For example, both riverine solutes used to estimate weathering fluxes (e.g. Gaillardet et al. (1999); Gaillardet et al. (2011); Meybeck (1987)) and sediment-gauging methods used to estimate rates of erosion (e.g. Ludwig et al. (1996); Milliman and Farnsworth (2011); Milliman and Syvitski (1992); Peucker-Ehrenbrink (2009); Pinet and Souriau (1988); Summerfield and Hulton (1994)) usually integrate over decades. Over weathering time scales, *in situ* cosmogenic nuclides can be used to quantify the denudation (i.e. the sum of weathering and erosion) of quartz-bearing lithologies. Measurements of *in situ* cosmogenic ^{10}Be from detrital quartz provide a well-established method to derive denudation rates for nearly all sizes of drainage basins (Bierman and Nichols, 2004; Granger and Schaller, 2014; von Blanckenburg, 2005; Wittmann and von Blanckenburg, 2016). For quartz-free lithologies, cosmogenic ^{3}He in olivine or pyroxene is the only possibility to constrain weathering and erosion over weathering time scales (Gayer et al., 2008; Puchol et al., 2017). However, olivine and pyroxene rarely survive extended periods of weathering. Hence, we still lack cosmogenic nuclide methods suitable for mafic lithologies.

Determining Earth surface rates with the "sister nuclide" of *in situ* ^{10}Be, the atmospherically produced meteoric ^{10}Be, does not depend on the presence of quartz (von Blanckenburg and Willenbring, 2014). Meteoric ^{10}Be is produced in the atmosphere at a rate known to a first order and reaches Earth´s surface by wet and dry deposition where it is adsorbed to any fine-grained solid material or is present in the dissolved form when pH and thus retentivity of Be is low (Willenbring and von Blanckenburg, 2010). When combined with the stable ^{9}Be counterpart, the trace metal Be that is released from bedrock during weathering, the resulting

^{10}Be(meteoric)/(stable)^{9}Be isotope ratio is a quantitative proxy for Earth surface processes (von Blanckenburg et al., 2012). The ratio depends on the ^{10}Be deposition rate, the ^{9}Be concentration of the parent bedrock, the fraction of ^{9}Be released from primary minerals, and the weathering front advance rate (Maher and von Blanckenburg, 2016), which at steady weathering zone thickness is interpreted as denudation rate (von Blanckenburg et al., 2012). The ^{10}Be/^{9}Be ratio can be determined either on the reactive phase of sediment (adsorbed onto or precipitated in secondary minerals), termed $(^{10}Be/^{9}Be)_{reac}$, or on the dissolved phase in stream water, termed $(^{10}Be/^{9}Be)_{diss}$. Therefore, this method is not restricted to a certain lithology. ^{10}Be adsorbed onto or incorporated into mineral phases can be released again under acidic conditions as its retentivity depends on pH values of soil and riverine solutions (Willenbring and von Blanckenburg, 2010).

In this study, we provide amongst the first cosmogenic nuclide-derived denudation rates for catchments underlain by (ultra-)mafic rocks by using the new ^{10}Be/^{9}Be system. We test the feasibility of this new weathering and erosion proxy on the scale of three creek-sized catchments (<1 km^2), all located in close proximity within the Slavkov Forest, NW-Czech Republic. This region was impacted by anthropogenic acid deposition in the second half of the 20th century. The studied catchments have similar topography, climate, vegetation, and catchment size, but exhibit contrasting lithologies ranging from felsic to mafic and ultramafic rocks, respectively. Due to this contrast in lithologies, pH values of stream waters vary from acidic to alkaline, displaying the ability of the mafic and ultramafic catchments to buffer the acidification caused by acid rain, while the felsic catchment is highly acidic with low acid-buffering capability. We determine erosion and denudation rates and the degree of weathering, and compare them with estimates by *in situ* cosmogenic ^{10}Be in quartz and with weathering rates from river load gauging. We also explore whether the depositional flux of ^{10}Be is in balance with the ^{10}Be flux exported in the sedimentary and dissolved form, and we suggest methods to derive catchment-representative ^{9}Be bedrock concentrations measured on deep drill core samples to avoid surficial alteration of concentrations.

1.1 Summary of the conceptual framework for simultaneously deriving erosion rates E, denudation rates D and degrees of weathering W

The cosmogenic meteoric nuclide ^{10}Be is now a versatile workhorse that is used for a multitude of Earth surface applications. Its concentration in soil and river particles has been used to e.g. date river terraces (Pavich et al., 1986) and glacial deposits (Ebert et

al., 2012; Egli et al., 2010) by using the “inventory method”, evaluate the steady state between atmospheric ^{10}Be delivery and its export in river sediment (Brown, 1988; You et al., 1988), riverine sediment mixing and source allocation (Belmont et al., 2014; Neilson et al., 2017), quantification of soil movement along slopes (Jungers et al., 2009; Mckean et al., 1993; West et al., 2013), general soil and weathering profile characterization (Graly et al., 2010), gully erosion (Portenga et al., 2017; Reusser and Bierman, 2010), or episodic erosion events from lake records (Valette-Silver et al., 1986). The calculation of erosion rates from river sediment, as done routinely using the *in situ* ^{10}Be variety in quartz, is rarely possible as meteoric ^{10}Be concentrations are highly grain-size dependent and are thus biased by hydrodynamic sorting (Wittmann et al., 2015).

In only very few studies the ^{10}Be/^{9}Be ratio was used for Earth surface applications: as tracer of river dissolved and particulate geochemistry (Brown et al., 1992), and as indicator of pedogenesis (Barg et al., 1997). To make use of this ratio for quantitative estimates of the rates of erosion (E), denudation (D), and the degree of gross weathering, a conceptual framework has been developed by von Blanckenburg et al. (2012). This framework offers the advantage in that the grain size dependencies affecting meteoric ^{10}Be in river sediment are removed by normalizing to the stable isotope ^{9}Be. The approach now allows to evaluate degrees of weathering and fluid/solid exchange of Be.

The concentration of ^{9}Be in bedrock, defined as $^{9}Be_{parent}$, continuously enters the weathering zone through advancement of the weathering front. Chemical weathering of bedrock and remaining primary minerals results in partial dissolution that leads to a mobilization of ^{9}Be and a fraction of ^{9}Be that remains locked in primary minerals, termed $^{9}Be_{min}$. Due to its particle-reactive nature, the mobilized ^{9}Be that is released during weathering eventually adsorbs onto mineral surfaces or is incorporated into precipitates, called “reactive” $^{9}Be_{reac}$. The ^{9}Be remaining in solution, called $^{9}Be_{diss}$, is exported as dissolved material. Reactive Be can be accessed via sequential chemical extraction (e.g. Wittmann et al. (2012)). Meteoric ^{10}Be enters the top of the weathering zone via wet and dry atmospheric deposition. Similarly to ^{9}Be, reactive ^{10}Be ($^{10}Be_{reac}$) adsorbs onto mineral surfaces or co-precipitates with Fe-Al-(hydr-)oxides or clays (von Blanckenburg et al., 2012). This ^{10}Be exchanges and most likely equilibrates with dissolved ^{10}Be through dissolution-precipitation or desorption-adsorption reactions.

From measuring single ^{10}Be concentrations and estimating the meteoric depositional flux of ^{10}Be to Earth´s surface, Brown et al. (1988) already calculated erosion rates.

Using the ^{10}Be mass balance approach presented below in combination with a retentivity correction (von Blanckenburg et al., 2012), erosion rates can be calculated according to:

$$E_{met} = \frac{\boldsymbol{F_{met}^{10Be}}}{\boldsymbol{[^{10}Be]_{reac}}} - \frac{q}{K_d} \quad (1a)$$

$$E_{met}{}' = \frac{\boldsymbol{F_{met}^{10Be}}}{\boldsymbol{[^{10}Be]_{reac}}} \quad (1b)$$

where E_{met} is the erosion flux (in kg m^{-2} y^{-1}), F_{met}^{10Be} is the atmospheric depositional flux of meteoric ^{10}Be (in ats m^{-2} y^{-1}), and $[^{10}Be]_{reac}$ is the ^{10}Be concentration in the reactive phase as determined by chemical extractions (in ats kg$_{solid}^{-1}$). Equation 1a shows that an accurate erosion rate can only be determined if the water runoff q (L m^{-2} y^{-1}) and the K_d value that describes the partition of an element between the particulate and the dissolved phase (in L kg^{-1}) are known over the residence time of meteoric ^{10}Be in the weathering zone (von Blanckenburg et al., 2012). Under certain conditions, i.e. for high retentivity of Be in the solid phase and low runoff, the right-hand term in eq. 1a can be ignored, yielding the simplified eq. 1b (E_{met}', in kg m^{-2} y^{-1}).

When the below-summarized isotope mass balances for ^{9}Be (eq. 3) and ^{10}Be (eqs. 4, 5) that assume equilibration between the dissolved and the reactive phase, are combined (von Blanckenburg et al., 2012), denudation rates can be calculated according to:

$$D_{met} = \frac{F_{met}^{10Be}}{\left(\frac{^{10}Be}{^{9}Be}\right)_{reac/diss} \times [\,^{9}Be]_{parent}} \times \left(\frac{[\,^{9}Be]_{min}}{[\,^{9}Be]_{reac}} + 1\right) - \frac{q}{K_d} \times \frac{[\,^{9}Be]_{min}}{[\,^{9}Be]_{parent}} \quad (2a)$$

$$D_{met}{}' = \frac{F_{met}^{10Be}}{\left(\frac{^{10}Be}{^{9}Be}\right)_{reac} \times [\,^{9}Be]_{parent} \times (f_{reac}^{9Be} + f_{diss}^{9Be})} \quad (2b)$$

$$D_{met^*} = \frac{F_{met}^{10Be}}{\left(\frac{^{10}Be}{^{9}Be}\right)_{reac/diss} \times [\,^{9}Be]_{parent}} \times \left(\frac{[\,^{9}Be]_{min}}{[\,^{9}Be]_{reac}} + 1\right) \quad (2c)$$

where D_{met} is the denudation rate (in kg m^{-2} y^{-1}), $(^{10}Be/^{9}Be)_{reac}$ is the ratio of ^{10}Be and ^{9}Be of chemically extracted Be, $[^{9}Be]_{parent}$ is the concentration of ^{9}Be in the unweathered bedrock (in ats kg$_{rock}^{-1}$), and the term $\left(f_{reac}^{9Be} + f_{diss}^{9Be}\right)$ quantifies the mobilized flux fraction of ^{9}Be that is released from primary minerals during weathering (see eq. 3 below). The simplified equations 2b, 2c ignore partitioning of Be into the dissolved phase and can be used in settings where retentivity of ^{10}Be is high in the solid phase. Equation 2c

furthermore introduces means to estimate the mobilized ^{9}Be flux fraction $\left(f_{reac}^{9Be} + f_{diss}^{9Be}\right)$ from sequential extractions of a single sediment sample. In contrast, river fluxes of dissolved and particular reactive ^{9}Be need to be known in equation 2b. Thus $(\mathrm{f_{reac}} + \mathrm{f_{diss}})$, can be calculated using the $[^{9}\mathrm{Be}]_{\mathrm{reac}}$ and $[^{9}\mathrm{Be}]_{\mathrm{min}}$ concentrations (both in g $\mathrm{kg_{solid}^{-1}}$) measured on river sediment, yielding $\left(f_{reac}^{9Be} + f_{diss}^{9Be}\right)_{\mathrm{min/reac}}$:

$$\left(f_{reac}^{9Be} + f_{diss}^{9Be}\right)_{\mathrm{min/reac}} = \frac{[\,^{9}\mathrm{Be}]_{\mathrm{reac}}}{[\,^{9}\mathrm{Be}]_{\mathrm{reac}} + [\,^{9}\mathrm{Be}]_{\mathrm{min}}} \quad (3)$$

Importantly, D from ^{10}Be/^{9}Be (eq. 2) is neither an erosion rate nor a sediment generation rate. Rather, it comprises the sum of erosion rate (physical denudation) and weathering rate (chemical denudation). In contrast, E from meteoric ^{10}Be (eq. 1) provides a true erosion rate. It does not account for chemical weathering and can hence provides a sediment generation rate.

1.2 Requirements for the successful application of the new proxy

A set of assumptions and prerequisites need to be met for applying this new proxy, and depending on setting, specific sampling strategies need to be designed. We provide a list of general (see von Blanckenburg et al., 2012) and site-specific requirements relevant for anthropogenically-affected creek-scale catchments with the aim to make the reader aware of the methods' requirements. We indicate the respective results and discussion sections in which we report our test of these assumptions in mafic catchments.

(1) Knowledge of the atmospheric ^{10}Be depositional flux over the residence time of the weathering zone. Derived erosion and denudation rates integrate over the residence time of ^{10}Be in the weathering zone (of the order of 10^4 ys). However, the depositional flux of meteoric ^{10}Be, $\mathrm{F}_{\mathrm{met}}^{^{10}\mathrm{Be}}$, varies with time both due to variations in magnetic field strength and daily fluctuations in precipitation patterns. Hence we need an estimate of depositional flux of meteoric ^{10}Be representative for similarly long time scales. This estimate cannot be reliably obtained from short-term precipitation records (Graly et al., 2011), but rather from meteoric ^{10}Be soil inventories of known age or erosion (e.g. Egli et al. (2010); Ouimet et al. (2015); Willenbring and von Blanckenburg (2010)), or time-averaged global circulation models. Here, we use a $\mathrm{F}_{\mathrm{met}}^{^{10}\mathrm{Be}}$ of 1.46×10^6 ats $\mathrm{cm^{-2}\ y^{-1}}$ derived from a combination of a model for the simulation of cosmic ray

particle interactions with the Earth's atmosphere (Masarik and Beer, 1999) with the "ECHAM5" fifth-generation global atmospheric circulation model (GCM) coupled to the aerosol model HAM (Heikkilä et al., 2013a; Heikkilä et al., 2013b). This model was run separately for the modern ("industrial") ^{10}Be deposition (Heikkilä et al., 2013a) and for the early Holocene ("pre-industrial") (Heikkilä et al., 2013b) and then these model runs were combined by averaging and accounting for changes in magnetic field strength (see Heikkilä and von Blanckenburg (2015), yielding a deposition rate that averages over the Holocene.

(2) Measuring a representative concentration of reactive meteoric ^{10}Be in sediment. $[^{10}Be]_{reac}$ needs to be obtained from sequential chemical extractions on a sample that is representative of the soil eroded in the entire catchment. $[^{10}Be]_{reac}$ however strongly depend on the measured grain size (Wittmann et al., 2012). In streams a grain size dependence arises from particle sorting that can introduce a bias on ^{10}Be concentrations due to i) smaller grains offering more surface area for adsorption (Maher and von Blanckenburg, 2016; Shen et al., 2004; Willenbring and von Blanckenburg, 2010); ii) larger grains containing more quartz that dilutes reactive Be (Bouchez et al., 2011; Wittmann et al., 2015); iii) the chemistry of adsorption sites differs with grain size (Wittmann et al, 2012; Singleton et al., 2017). The most reliable approach to determine such representative concentrations is from river depth profiles when the depth-integrated mean grain size transported by the river is known (Wittmann et al., 2015). For small streams where this is not possible, it may be advisable to use a bulk sediment sample or to analyze different grain size fractions. In this paper, we use a "bulk" estimate (<500 µm fraction) of the ^{10}Be concentration as best estimate (see section 5).

(3) Knowledge of partitioning of Be between the solid and the dissolved phase. At low pH values (<6), a fraction of Be is removed in the dissolved form. If this fraction is significant, it needs to be accounted for when estimating erosion rates (eq. 1) or denudation rates (eq. 2). If river runoff q is known, this correction can be done by pH measurement and from empiric relations between pH and partitioning factor K_d (e.g. You et al., 1989). For anthropogenically-affected catchments where the acidic pH is still recovering from the acid rain period such as in the Lysina catchment, one must know a long-term, pre-acidification pH value, for example from observation-based hydrological modelling (e.g. see Hruška and Krám (2003)). We explore this requirement in detail in section 6.1 for the study area.

(4) $(^{10}Be/^{9}Be)_{reac}$ is representative of $(^{10}Be/^{9}Be)_{diss}$. If a significant fraction of the Be flux is present in the dissolved form, then attainment of equilibrium between $(^{10}Be/^{9}Be)_{reac}$ and $(^{10}Be/^{9}Be)_{diss}$ is a prerequisite to close the mass balance. Given the

small spatial scale of our catchments that might preclude spatial homogenization of ^{10}Be and ^{9}Be between the reactive and the dissolved pools, we explore this requirement in detail in section 6.2.

(5) Balance between atmospheric ^{10}Be deposition flux and river output flux. A prerequisite for applying the mass balance approach for ^{10}Be is that the inputs of ^{10}Be into a drainage basin, derived from knowing the depositional flux, balance the outputs of ^{10}Be, by export from riverine and dissolved fluxes (von Blanckenburg et al., 2012). The basin-wide atmospheric input of ^{10}Be, $J_{atm}^{^{10}Be}$, in ats y^{-1}, is given by $F_{met}^{^{10}Be}$, the depositional flux of meteoric ^{10}Be to the Earth's surface (in ats m^{-2} y^{-1}) that reaches the catchment´s surface area A_{riv} (in m^2) (after Wittmann et al., 2015):

$$J_{atm}^{^{10}Be} = A_{riv} \times F_{met}^{^{10}Be} \quad (4)$$

The total meteoric flux of ^{10}Be exported by the riverine system, $J_{riv}^{^{10}Be}$, in ats y^{-1}, is given by:

$$J_{riv}^{^{10}Be} = J_{riv-reac}^{^{10}Be} + J_{riv-diss}^{^{10}Be} = \left[\left(A_{riv} \times E \times \left[^{10}Be\right]_{reac} + Q \times \left[^{10}Be\right]_{diss}\right) \times \left(1 - \exp^{(-\lambda t(i))}\right)\right] \quad (5)$$

where $J_{riv-reac}^{^{10}Be}$ and $J_{riv-diss}^{^{10}Be}$ are the riverine solid reactive (adsorbed and secondary solids) and dissolved fractions transported by the river (in ats y^{-1}), respectively. These can be calculated from the catchments area A_{riv} and its reactive and dissolved concentrations, $[^{10}Be]_{reac}$ (in ats kg_{solid}^{-1}) and $[^{10}Be]_{diss}$ (in ats L^{-1}), multiplied by an independently-derived erosion rate E (in kg m^{-2} y^{-1}, i.e. from sediment gauging or *in situ* ^{10}Be), and the catchments discharge Q (in L yr^{-1}), respectively. The right-hand term in equation 5 describes the radioactive decay of ^{10}Be during sediment transfer and storage with the decay constant λ (5×10^{-7} y^{-1} corresponding to a half-life of 1.39 My, e.g. Chmeleff et al. (2010); Korschinek et al. (2010)). The balance of ^{10}Be fluxes is attained if $J_{riv}^{^{10}Be} = J_{atm}^{^{10}Be}$ (Wittmann et al., 2015). We explore this balance in section 7.2.

(6) The catchment-wide concentration of $[^{9}Be]_{parent}$ is known. Required as an essential input for estimating D (eq. 2), $[^{9}Be]_{parent}$ can be estimated for large basins as spatial averaging of rock type is ensured from published summaries of Be concentrations in the prevailing bedrock types. For example, von Blanckenburg et al. (2012) proposed to use the mean crustal average Be concentration of 2.5 ppm for felsic

crystalline or clastic sedimentary lithologies. However, in small basins, and especially in mafic settings, $[^9Be]_{parent}$ needs to be obtained from measuring local bedrock samples. Hence the minimum requirement is to carry out thorough characterization of surface lithologies for their ^9Be concentrations. In section 8.1, we explore this requirement for the studied catchments and suggest correlation methods and statistical means to derive meaningful concentrations where bedrock is very heterogeneous.

(7) A representative weathering fraction $\left(f_{reac}^{9Be} + f_{diss}^{9Be}\right)$ can be determined. As the ratio $\frac{[\,^9\mathrm{Be}]_{\mathrm{min}}}{[\,^9\mathrm{Be}]_{\mathrm{reac}}}$ that is used to calculate the Be-specific weathering fraction $\left(f_{reac}^{9Be} + f_{diss}^{9Be}\right)$, an input for estimating D (eq. 2), may also be biased from particle sorting, this bias can propagate into the derived denudation rates (Rahaman et al., 2017). Because $\frac{[\,^9\mathrm{Be}]_{\mathrm{min}}}{[\,^9\mathrm{Be}]_{\mathrm{reac}}}$ mostly varies over a narrow range, this bias is not overly large. Still, sampling representative grain sizes or river depth-profiles ensures reduction of this bias. In section 8.2, we explore means to estimate this value.

2. Study area

The Slavkov Forest is located in western Bohemia in the northwest of the Czech Republic (see Fig. 1). Geologically the area of the Slavkov Forest is dominated by the Karlovy Vary Massif, a Late Variscan granite body (Blecha and Štemprok, 2012). In the south of the Slavkov Forest, mafic rocks of the Mariánské Lázně Complex, a high-grade ophiolitic complex, occur (Jelínek et al., 1997). The felsic Lysina catchment (LYS) is underlain by leucocratic granite comprising orthoclase, quartz, albite and a lithium mica as main minerals (Navrátil, 2000; Štědrá et al., 2016). In the other catchments that are located in the direct vicinity of Lysina, mafic and ultramafic rocks of the Mariánské Lázně Complex crop out. The mafic Na Zeleném catchment (NAZ) exhibits mainly retrogressed garnetiferous amphibolite with intrusions of Mg-rich metadorite (Štědrá et al., 2015). The amphibolite predominantly consists of tremolite and plagioclase. The ultramafic Pluhův Bor catchment (PLB) is dominated by serpentinite, tremolite schist and actinolitic schist, and amphibolites (Krám et al., 2009). The predominant mineral in the serpentinite is antigorite with trace amounts of opaque minerals and talc (Krám and Hruška, 1994; Krám et al., 2012). In the Pluhův Bor catchment, veins containing quartz are present.

All catchments have similar topography, altitude, catchment size, mean annual air temperature (5-6 °C), mean precipitation of about 950 mm (Table 1), and similar

vegetation (mainly spruce). The catchments are 0.22 - 0.55 km^2 in size with perennial 1st order streams of less than one-kilometer length. Mean slopes are 5-15%. Due to the different bedrock types the stream waters reveal highly contrasting hydrochemical characteristics and highly differentiated stream chemistry regarding their cation load (Krám et al., 2012). In the second half of the 20th century, atmospheric anthropogenic acid deposition affected European terrestrial and aquatic ecosystems, causing soil acidification and local acidification of surface waters (Drever, 1997; Pačes, 1985; Reuss et al., 1987). In the felsic Lysina catchment, anthropogenic acidification resulted in acidic soil and stream waters. The soil water pH in the (ultra)mafic catchments is slightly acidic in the uppermost organic and mineral horizons but neutral to alkaline in C horizon and stream water (Krám et al., 2013). The stream water in Lysina is characterized by a very low mean pH value of 4.2 and a negative alkalinity. The chemistry of the Lysina stream water is dominated by Ca-Na-SO_4-organic acids and elevated Al concentrations, characteristic for acidic waters (Krám et al., 2012). The stream water in the mafic Na Zeleném catchment is neutral (pH ~6.9), has a moderate alkalinity and a solute composition characterized by Ca-Mg-SO_4-HCO_3. Stream water in the ultramafic Pluhův Bor catchment has the highest pH values (~7.6) and alkalinity. The predominant components are Mg-HCO_3-SO_4-organic acids and elevated concentrations of SiO_2, Ni and Cr are apparent (Krám et al., 2012).

3. Sampling and sample types

We sampled bedload sediment and stream water at the outflow of each catchment in August 2011; in addition, stream water samples from a period of 2012 to 2013 were analysed, for which we present average values (section 5.4). From the Lysina catchment we additionally sampled groundwater from the shallow “Lenka” well (Fig. 2). Because upland mountain bedrock outcrops contain highly weathered rock throughout, sampling fresh bedrock for estimating the ^9Be bedrock concentration and its variability is virtually impossible. To obtain such samples, we thus used drill core samples. In August/September 2012, cores were taken within the framework of the SoilTrEC project (Menon et al., 2014; Regelink et al., 2015). The final depth was 30.3 m at Lysina, 26.1 m at Na Zeleném, and 28.0 m at Pluhův Bor. From all three cores, specimens of bedrock were sampled. The top part of the Lysina core that contains soil and sediment, was also sampled (except the uppermost organic rich part), down to the sediment-bedrock interface at 3.4 m depth. Note that we cannot exclude vertical mixing of sampled material in the uppermost meters of the soil.

4. Methods

4.1 Bedload, bedrock, and drill core samples

Prior to chemical extraction, bedload sediment samples were manually dry-sieved into a fraction <63 µm. We used mainly this fraction for ^{10}Be extraction (see Table 2). In addition, we explored the dependence of beryllium concentrations on grain size by further determining $[^{9}Be]_{reac}$ on coarser grain size fractions (63-125 µm, 125-250 µm, and 250-500 µm) of bedload sediments (Table 3; Fig. 3); $[^{10}Be]_{reac}$ was additionally measured on 125-250 µm grain size fraction (Table 2), and the $[^{10}Be]_{reac}$ of a "bulk" (<500 µm) sediment composition was calculated (Table 3).

Chemical extraction of reactive ^{10}Be and ^{9}Be from bedload sediment was performed under clean lab conditions following the method of Wittmann et al. (2012), i.e. the successive steps of amorphous oxide ("am-ox") and crystalline oxide ("x-ox") leaches were in most cases combined to a "reactive" fraction. Individual data for am-ox and x-ox leaches is available for the fine-grained (<63 µm) bedload fraction (Fig. 3; Supplementary Table S1). The solid sample residuals of chemical leaches were decomposed using mixtures of hydrofluoric acid (HF) and aqua regia to derive the mineral-bound Be_{min}. After complete dissolution and/or chemical extraction, splits of solutions were spiked with ^{9}Be carrier and then the Be was purified using column chemistry, alkaline precipitation and oxidation to BeO following established methods (e.g. von Blanckenburg et al. (1996)). ^{9}Be analysis was performed using *Inductively Coupled Plasma-Optical Emission Spectroscopy* (ICP-OES, Varian 720ES) on splits of solutions before carrier addition. ^{10}Be analysis was performed using *Accelerator Mass Spectrometer* (AMS) at Cologne University relative to standards KN01-6-2 (5.35×10^{-13}) and KN01-5-3 (6.32×10^{-12}) (Dewald et al., 2013) or ETH Zurich where the measured ^{10}Be/^{9}Be ratios were normalized to the ETH in house standard *S2007N* with a nominal ratio of 28.1×10^{-12} (Christl et al., 2013).

Splits of bedload samples were additionally processed for *in situ* cosmogenic ^{10}Be in quartz using the above-described methods (carrier addition, column chemistry, alkaline precipitation, oxidation and AMS measurements) after quartz purification. For Lysina bedload, the 250-500 µm and 500-800 µm fractions were used, and for Na Zeleném and Pluhův Bor bedload, the composite 125-800 µm fraction was used due to very low amounts of quartz in these samples. ^{10}Be concentrations were calculated from the normalized and blank corrected ^{10}Be/^{9}Be ratios. Reported 1 sigma uncertainties include counting statistics, the variability of the ^{10}Be/^{9}Be ratio during repeated measurements of

the same sample, and the uncertainties of both, standard normalization and blank correction.

All bedrock samples from the drill cores were characterized petrographically (Supplementary Table S2). Parent beryllium concentrations ($[^{9}Be]_{parent}$) were determined from pieces of the bedrock cores. The samples were crushed and 100-200 mg bulk aliquots were digested using HF/aqua regia mixtures. The bedrock beryllium concentration measurements were performed using ICP-OES. Concerning the ultramafic samples, the beryllium concentration was in some cases below the detection limit of the ICP-OES, which is ca. 10 ppb for Be.

From the Lysina core, we processed five regolith samples sieved to <2 mm from the upper 3.4 m part and one sample comprising weathered fragments of broken bedrock from a depth of 4.4 m. This sample was ground before chemical leaching. These samples were analyzed for ^{10}Be and ^{9}Be in the combined reactive and the mineral-bound phases using the above-described methods.

X-ray fluorescence (XRF) analyses were carried out on all bedload, bedrock, and regolith samples to determine the major and trace elemental concentrations (see supplementary Tables S3 for bedrock core, S4 for bedload). Prior to bedrock analysis, the samples were crushed (bedrock) and powdered, followed by preparation of fusion tablets for XRF analysis. The XRF analyses were carried out with a *PANanalytical Advance* at GFZ Potsdam.

4.2 Water samples

Stream and ground water samples were filtered through a 0.2 µm membrane filter and acidified with nitric acid to a pH of 1-2 on the day of sampling. Samples were then separated into two splits, where one subsample was used for *sector-field High-Resolution Inductively Coupled Plasma-Mass Spectrometry* (HR-ICP-MS, ThermoFisher Element 2) for ^{9}Be analysis and another was used for ^{10}Be analysis by AMS after spiking with a ^{9}Be carrier and separation of Be (Wittmann et al., 2015). An iron chloride ($FeCl_3$) solution was added to the AMS sample portions to co-precipitate Be with ferric hydroxide (an approach adapted from Jeandel (1993) and Frank et al. (2009) developed for ocean water). We used about 200 to 600 mL of stream water for ^{10}Be analysis (Supplementary Table S5), which were mainly carried out at AMS facility of Cologne University.

Very low ^{9}Be concentrations of the stream water of the two mafic catchments made pre-concentration of samples necessary; about 50 mL of water were evaporated and taken up again in weak nitric acid for HR-ICP-MS measurements. In case of visible high

dissolved organic carbon content, the samples were fumed with concentrated H_2O_2 and HNO_3. The full analytical procedure is given in Wittmann et al. (2015).

5. Results

5.1 ^{10}Be and ^{9}Be concentrations of bedload samples

For all samples where amorphous oxide and crystalline oxide fractions were determined separately (i.e. the <63 µm of bedload samples, Table S1), the am-ox fraction yields higher [^{9}Be] by a factor of two to four than the x-ox fraction (see Fig. 3). Residual mineral-bound ^{9}Be ($[^{9}Be]_{min}$) concentrations are higher than $[^{9}Be]_{reac}$ in the Lysina catchment, where $[^{9}Be]_{reac}$ comprises about ~26% of $[^{9}Be]_{total}$ ("total" being the sum of $[^{9}Be]_{reac}$ + $[^{9}Be]_{min}$; note that "total" is not the same as "parent" due to loss of soluble elements from regolith and sediment). In contrast, the sediments of the other catchments have higher ^{9}Be concentrations in the reactive than in the mineral-bound phase (NAZ: $[^{9}Be]_{reac}$ ~63% of $[^{9}Be]_{total}$; PLB: $[^{9}Be]_{reac}$ ~54% of $[^{9}Be]_{total}$; Table 2). The apportionment of ^{10}Be between the extracted phases is similar to ^{9}Be, with $[^{10}Be]_{am\text{-}ox}$ being higher by a factor of six to eight than $[^{10}Be]_{x\text{-}ox}$ in fine-grained bedload samples (Table S1). Summed $[^{10}Be]_{reac}$ of the Na Zeleném and Pluhův Bor catchments are similar with $(400\pm11)\times10^{6}$ ats g^{-1} and $(403\pm11)\times10^{6}$ ats g^{-1}, respectively, and are about $(177\pm5)\times10^{6}$ ats g^{-1} for the granitic Lysina catchment. Mineral-bound fractions of [^{10}Be] ($[^{10}Be]_{min}$) comprise only 2-8% of total ^{10}Be.

Regarding $(^{10}Be/^{9}Be)_{reac}$ ratios, the fine-grained bedload of Lysina and Na Zeleném both yield low ratios of $(18\pm1)\times10^{-10}$ and $(28\pm1)\times10^{-10}$, respectively (Table 2), whereas $(^{10}Be/^{9}Be)_{reac}$ measured at Pluhův Bor is with $(194\pm10)\times10^{-10}$ comparably high, due to the very low ^{9}Be concentrations. All three catchments reveal lower $(^{10}Be/^{9}Be)_{x\text{-}ox}$ than $(^{10}Be/^{9}Be)_{am\text{-}ox}$ ratios (Fig. 3).

When comparing the <63 µm to the 125-250 µm size fractions, single $[^{10}Be]_{reac}$ and $[^{9}Be]_{reac}$ decrease markedly with increasing grain size. In contrast, calculated $(^{10}Be/^{9}Be)_{reac}$ for these two grain size fractions are almost identical within the analytical uncertainty (Table 2, Fig. 3). To obtain single $[^{10}Be]_{reac}$ that are more representative of bulk (<500 µm) sediment transport (see section 1.2), we first calculated an average $(^{10}Be/^{9}Be)_{reac}$ ratio from the two values measured on the <63 and 125-250 µm size fractions. As this ratio is independent of grain size, we then multiplied the average $(^{10}Be/^{9}Be)_{reac}$ ratio with individual $[^{9}Be]_{reac}$ (obtained for all grain size fractions) to derive a $[^{10}Be]_{reac}$ for the respective grain size (Table 3). Note that these recalculated $[^{10}Be]_{reac}$ slightly differ from those actually measured on the <63 and 125-250 µm size fractions, because we used the averaged (^{10}Be/^{9}Be) for calculation. To obtain bulk-$[^{10}Be]_{reac}$ we then multiplied the recalculated $[^{10}Be]_{reac}$ with the fractional amount of each grain size

(Table 3), derived from weighting each grain size fraction after sieving, and summed these. From this last step, also bulk-$[^{9}Be]_{reac}$ were calculated.

5.2 ^{10}Be and ^{9}Be concentrations for Lysina core samples

A general trend in the core is that $[^{10}Be]_{reac}$ decreases with increasing depth whereas $[^{9}Be]_{reac}$ is increasing (Fig. 4, Table 4). The highest $[^{10}Be]_{reac}$ of 97×10^{6} ats g^{-1} is measured in the middle part of the profile at ca. 150 cm depth, such that the profile exhibits a slight "bulge" shape (Fig. 4). The $[^{10}Be]_{reac}$ in the deepest sample (from highly fractured and weathered bedrock) is ca. 17×10^{6} ats g^{-1}. This concentration comprises ca. 20% of the concentration measured in the uppermost sample of the core. The $[^{9}Be]_{reac}$ ranges from between 480 to 730 ng g^{-1}, with the highest $[^{9}Be]_{reac}$ measured at a depth of ca. 220 cm. $(^{10}Be/^{9}Be)_{reac}$ decreases continuously throughout the profile. A ratio of ca. 22×10^{-10} is measured for the uppermost sample that decreases with depth to a ratio of ca. 5×10^{-10} (Fig. 4).

5.3 ^{9}Be concentrations for bedrock samples

In order to determine spatially-representative $[^{9}Be]_{parent}$, we measured bedrock samples from different depths of each of the drill cores. From the mineralogical characterization of the cores (Table S2), we note a large heterogeneity regarding lithology in the catchments. Correspondingly, the beryllium concentrations of bedrock ($[^{9}Be]_{bedrock}$) among individual catchments (Fig. 5) and individual bedrock types (Table 5) are highly heterogeneous.

Beryllium concentrations of the parent bedrock ($[^{9}Be]_{parent}$, in μg g^{-1}) vary by an order of magnitude in the granitic Lysina catchment (from 2.8 μg g^{-1} up to about 20 μg g^{-1}; Table 5). The average $[^{9}Be]_{parent}$ of the granite is about 5.4 μg g^{-1} and the median value is about 3.5 μg g^{-1} (Fig. 5). Amphibolites of the Na Zeleném catchment have an average $[^{9}Be]_{parent}$ of ca. 0.69 μg g^{-1}. The metabasites and -dolerites found in this catchment (Table S2) yield, with an average 2.5 μg g^{-1}, markedly higher $[^{9}Be]_{parent}$. The ultramafic serpentinite at Pluhův Bor has low $[^{9}Be]_{parent}$ of less than 10 ng g^{-1}. In contrast, the amphibolites and metabasites prevailing in Pluhův Bor yield, relative to the ultramafic rocks, higher Be concentrations of 0.5 μg g^{-1} and 0.2 μg g^{-1}, respectively (Table 5). In Section 8.1, we discuss several potential ways of deriving catchment-average values for $[^{9}Be]_{parent}$ as determining these values accurately is crucial for deriving accurate denudation rates.

5.4 ^{10}Be and ^{9}Be concentrations for water samples

The dissolved meteoric ^{10}Be concentrations are highest in the acidic Lysina catchment (2-year average $[^{10}Be]_{diss}$ with 1SD of dataset = (11.8 ± 1.7)×10^4 ats g^{-1}, n = 10, Table 6). $[^{10}Be]_{diss}$ measured in one groundwater sample in the Lysina catchment is with 13.4 ± 0.4 ats g^{-1} similar to the stream water. The 2-year average $[^{10}Be]_{diss}$ (n = 10) in the neutral Na Zeleném catchment is (1.02 ± 0.75)×10^4 ats g^{-1} and in the alkaline catchment Pluhův Bor, the 2-year average of $[^{10}Be]_{diss}$ is (2.1 ± 1.8)×10^4 ats g^{-1} (n = 10, Table 6). For these two catchments no $[^{10}Be]_{diss}$ in groundwater is available.

For the same sample set, average dissolved [^{9}Be] are highest for the stream water in Lysina (969 ± 82 ng L^{-1}, Table 6). $[^{9}Be]_{diss}$ is distinctly higher in the Lysina groundwater (2075 ± 161 ng L^{-1}) than in the stream water although the pH of the groundwater is less acidic. In the Na Zeleném and Pluhův Bor catchments, $[^{9}Be]_{diss}$ of stream waters are almost two orders of magnitude lower compared to Lysina (2-year average $[^{9}Be]_{diss}$ = 25 ± 14 ng L^{-1} for NAZ and 17 ± 11 ng L^{-1} for PLB; Table 6, each n = 10).

The ^{10}Be/^{9}Be ratio of dissolved beryllium ($(^{10}Be/^{9}Be)_{diss}$) is in Lysina on average (18.4 ± 3.0)×10^{-10}, in Na Zeleném (57 ± 11)×10^{-10}, and Pluhův Bor reveals the highest ratio of (168 ± 50)×10^{-10}. $(^{10}Be/^{9}Be)_{diss}$ of the groundwater in Lysina is (9.64 ± 0.82)×10^{-10} (Table 6).

5.5 *In situ*-^{10}Be derived denudation rates from bedload samples

In the felsic Lysina catchment, the *in situ*-produced ^{10}Be concentration is uniform for the two analyzed grain sizes (17.7×10^4 ats g^{-1}; Table 7). Similar *in situ*-cosmogenic ^{10}Be concentrations of 17.9×10^4 ats g^{-1} are found in the mafic Na Zeleném catchment. In the ultramafic Pluhův Bor catchment, where quartz minerals are mainly found in veins, we find a higher *in situ*-produced ^{10}Be concentration of 33.8×10^4 ats g^{-1}. Since the *in situ*-^{10}Be production rate of these catchments (Table 7) is almost identical due to similar topography and latitude, these nuclide concentrations scale in accordance to their D_{insitu}: 101 t km^{-2} y^{-1} (≙39 mm ky^{-1}) on average for the felsic Lysina and 91 t km^{-2} y^{-1} (≙35 mm ky^{-1}) for the mafic Na Zeleném, whereas the ultramafic Pluhův Bor catchment exhibits a lower denudation rate of 46 t km^{-2} y^{-1} (≙17.5 mm ky^{-1}). These *in situ*-derived denudation rates integrate over the time it takes to erode one attenuation path length that is the depth at which 1/*e* of the incoming cosmic rays are attenuated (e.g. von Blanckenburg, 2005). In bedrock this length is equal to 60 cm. The integration time scales are thus ≙15 ky in Lysina, ≙17 ky in Na Zeleném, and ≙34 ky in Pluhův Bor (Table 7).

6. Exploring fluid - solid interaction with ^{10}Be and ^{9}Be

6.1 Retentivity and partition coefficients of beryllium

The K_d value describes the partitioning of an element between the solid and the dissolved phase (in L kg^{-1}). Knowing the K_d value of Be is required for the calculation of erosion and denudation rates (section 9) if a significant flux fraction of Be is removed in the dissolved form. One means (i) to determine a catchment-specific K_d is through measuring ^{9}Be or ^{10}Be concentrations in the (ideally paired) dissolved and reactive Be phases:

$$K_d = \frac{[Be]_{reac}}{[Be]_{diss}} \quad (6)$$

Another means (ii) is to estimate K_d if a long-term pH (corresponding over the time scale within ^{10}Be has accumulated in the weathering zone) is known. K_d values can then be read from empiric relations between pH and K_d (e.g. You et al., 1989). For settings affected by industrial acidic precipitation, K_d values determined using approach (i) would lead to values representing the period of acid rain but not a weathering time-scale integrated condition. This is currently the case in the Lysina catchment because the pH is still recovering after the acid rain period of the last century (Hruška and Krám, 2003). Similarly, regarding approach (ii), one must know a long-term, pre-industrial pH value.

For the (ultra-)mafic catchments, the so-called *MAGIC* model (Model of Acidification of Groundwater in Catchments, see Hruška and Krám (2003)) predicts that annual mean stream water pH was at no period below 6.8 (Hruška and Krám, 2003). Accordingly, measured (approach (i)-derived) K_d values for ^{10}Be are 6.1×10^4 L kg^{-1} at Na Zeleném and 2.7×10^4 L kg^{-1} at Pluhův Bor, respectively (Table 8). These K_d values are in the range of experimental data obtained for ^{7}Be under controlled laboratory conditions for river sediment and specific clay mineral phases by You et al. (1989). Regarding the acidic Lysina catchment, the measured K_d value for ^{10}Be is low (1.3×10^3 L kg^{-1}) (section 6.2, Table 8). A similarly low K_d values arises from approach (ii) for a present-day pH value of 4.2 at Lysina (Table 8). If we use a simulated pre-industrial pH value of 5.5 (Hruška and Krám, 2003), we estimate a K_d value of 1.5×10^4 L kg^{-1}. This K_d value should adequately reflect, on times scales of erosion and weathering, the interaction of the dissolved phase with the long-term reactive Be pool.

6.2 Chemical equilibrium of $(^{10}Be/^{9}Be)_{diss}$ and $(^{10}Be/^{9}Be)_{reac}$

To assess fulfilment of requirement (4) in section 1.2, we compare $(^{10}Be/^{9}Be)_{diss}$ to $(^{10}Be/^{9}Be)_{reac}$. In Lysina, $(^{10}Be/^{9}Be)_{diss}$ is on average 18.4×10^{-10} over a period of two years (Table 6) and equals $(^{10}Be/^{9}Be)_{reac}$ in any grain size of the bedload sediment (Table 2). In the mafic Pluhův Bor and the ultramafic Na Zeleném catchments, $(^{10}Be/^{9}Be)_{reac}$ and $(^{10}Be/^{9}Be)_{diss}$ are within a factor of about two. To explore these processes in more detail, we inspect the potentially different equilibration behaviour of the amorphous vs. crystalline oxide fractions. At the time of paired sampling of bedload and stream water in August 2011, $(^{10}Be/^{9}Be)_{diss}$ are closer to those ratios measured in the amorphous fraction than compared to those ratios determined on the crystalline oxide fraction (Fig. 6). A similar observation was made by Wittmann et al. (2015) on the much larger spatial scale in the Amazon River and was attributed to early formation of crystalline oxides in the weathering zone, and preferential equilibration between amorphous oxides with dissolved phases during river transport and floodplain storage, respectively. Compared to crystalline structures these amorphous particles have large reactive surface areas and sorption and surface precipitation are rapid (Waychunas et al., 2005). In a recent sequential leaching study a similar dependence of $(^{10}Be/^{9}Be)_{reac}$ on the chemistry of reactive surfaces was found (Singleton et al., 2017). Amorphous oxides convert into crystalline oxides by crystallisation within the aggregate structure of the amorphous oxides (Schwertmann et al., 1999). As the degree of crystallization increases with pedogenetic time (Cudennec and Lecerf, 2006), crystalline oxides likely inherit a dissolved ($^{10}Be/^{9}Be$) signal from the time of formation of the amorphous oxides and thus preserve the memory of an early pedogenetic stage, or a different depth. $(^{10}Be/^{9}Be)_{reac}$ at deeper depths of a soil profile are expected to be lower (Maher and von Blanckenburg, 2016) and crystalline oxides formed at these depths will preserve ratios from variable depths during movement towards the surface as the soil is being eroded.

7. Evaluating geomorphic steady state conditions and its effects on the balance of meteoric ^{10}Be input and output fluxes

7.1 Are the watersheds in geomorphic steady state?

The mass balance framework of von Blanckenburg et al. (2012) and related calculations of erosion and denudation rates rely on the prerequisite that the landscape

is “at steady state” (requirement 5 in section 1.2). What this means is that erosion and denudation rate are quasi steady within a few method averaging time scales, defined by the depth of *in situ* or meteoric cosmogenic ^{10}Be occurrence divided by denudation rate (von Blanckenburg, 2005; Willenbring and von Blanckenburg, 2010). *In situ* ^{10}Be-derived integration time scales are 15 kys for Lysina, 17 kys for Na Zeleném, and 34 kys for Pluhův Bor (Table 7). For meteoric ^{10}Be, an averaging time scale can be calculated from the inventory of ^{10}Be (Table 4) following Willenbring and von Blanckenburg (2010), which denotes to 24.5 kys in Lysina. Note that since there are significant amounts of ^{10}Be still present at depth of >4 m (Table 4), and a substantial loss of ^{10}Be occurred into the dissolved load, this averaging time scale for Lysina is a minimum estimate. In absence of inventories for Na Zeleném and Pluhův Bor, the approach combining denudation rate and percolation depth (Willenbring and von Blanckenburg, 2010) can be used, resulting in 21 kys in Na Zeleném and 20 kys in Pluhův Bor when using soil depths of 90 cm and 120 cm (Table 1) and denudation rates from section 9.2, respectively. An alternative way to interpret cosmogenic ^{10}Be concentrations that does not rely on steady state of denudation time is that they represent an age, set by accumulation of nuclides since an event that “zeroed” cosmogenic nuclide concentrations. In European upland watersheds like the Slavkov Forest that have not been glaciated in the last glacial maximum (LGM), such zeroing potentially has occurred by removing the previously accumulated ^{10}Be by periglacial hillslope transport (Raab et al., 2007) and Pleistocene permafrost (Czudek, 1993). In that case the calculated time scales are exposure ages (Lal, 1991). However, we note that our minimum meteoric ages exceed the 15 to 20 kys expected for periglacial resetting during the LGM. Second, when comparing to those from *in situ* ^{10}Be (which would also be affected by zeroing of the landscape), these ages are too non-uniform to be explained by a single resetting event that in any case would have required removal of several meters of saprolite. We therefore discount these concentrations to represent ages of a landscape.

Still, these averaging time scales encompass the transition from the last cold stage into the Holocene, which might have involved changes in erosion rate of which cosmogenic nuclides retain a memory (Schaller et al., 2002a). Climatic factors such as shifts in precipitation or evapotranspiration and related changes in vegetation coverage or soil exposure have also been invoked from discharge models as cause for differences between *in situ* cosmogenic nuclide denudation rates and those from river load gauging (Meyer et al., 2010). Partial removal including downhill transport of periglacial slope deposits would result in perturbed vertical concentration profiles (Schaller et al., 2002a).

We note, however, that the depth profile in the Lysina core (Fig. 4b) shows the expected increase in $^{10}Be/^{9}Be$ towards the surface (Maher and von Blanckenburg, 2016), arguing against a massive perturbation. Thus, even though we have sufficient evidence to discount a wholesale resetting of the landscape during LGM we cannot assess whether full steady state has been attained either. Fortunately, the balance between depositional fluxes of meteoric ^{10}Be and export fluxes is also an indication of landscape steady state. We proceed to evaluate this balance.

7.2 ^{10}Be flux balance results

We calculate according to eq. 4 the flux of atmospheric meteoric ^{10}Be deposited at the surface area of a catchment (J_{atm}^{10Be}) and according to eq. 5 the dissolved plus reactive meteoric ^{10}Be flux exported in the dissolved and particulate form, respectively, via streams (J_{riv}^{10Be}), and compare the two with each other. Since we do not know the representative grain size exported from our catchments, we use our "bulk" estimate (<500 µm fraction) of the ^{10}Be concentration (termed $[^{10}Be]_{bulk}$, in ats g^{-1}) from Table 2 as best estimate in eq. 5. Further, $J_{riv\text{-}reac}^{10Be}$ requires knowing the sediment flux E that carries reactive ^{10}Be. Because sediment gauging has not been done in the Slavkov Forest we calculated the sediment flux from the *in situ* ^{10}Be-derived denudation rates (Table 7). However, as D_{insitu} is a measure of both weathering and erosion we subtracted the weathering flux by assuming a 50% weathering contribution to total denudation. This estimate is justified for granitic lithologies (whereas it may underestimate weathering degrees for mafic lithologies that contain only minor amounts of quartz) as the chemical depletion factor (CDF), a measure of weathering, is 0.5 in most supply-limited weathering zones (Dixon and von Blanckenburg, 2012) such as the Slavkov Forest. Further, as discussed in the preceding section, the estimate of D from *in situ* ^{10}Be might be affected by partial non-steady state behaviour, and might overestimate E if erosion was higher in LGM times than today. We cannot circumvent this issue, and attribute a maximum uncertainty of 50% to the combination of these two assumptions.

Bearing these caveats in mind, the exported to depositional flux ratio, $J_{riv}^{10Be}/J_{atm}^{10Be}$ (Table 9), scatters around a value of 1, indicating steady state regarding the ^{10}Be flux, for the mafic and ultramafic catchments. With a value of 3.0, $J_{riv}^{10Be}/J_{atm}^{10Be}$ for the felsic Lysina catchment is distinctly above 1. This high value of J_{riv}^{10Be} is dominated by very high

export of ^{10}Be in the dissolved phase (Table 9). Regarding the chemical state of the Lysina catchment (i.e. low acid buffering capacity, acidic pH), an excessive present-day export of ^{10}Be in the dissolved phase is anticipated given that K_d values are pH-dependent. If we use a long-term pH estimate and a respective higher K_d value for Lysina (given in Table 8) to correct for the loss of ^{10}Be to the dissolved phase, resulting $J_{riv}^{^{10}Be}/J_{atm}^{^{10}Be}$ is 0.6 (Table 9), being much closer to a value of 1. To have further re-assurance that the present-day loss of ^{10}Be in the dissolved phase is a recent phenomenon, we have assessed the impact of watershed acidification on the inventory of the long-term reactive ^{10}Be pool (Table 4). We calculate (Text S1 in the Supplement) a "lost" inventory since watershed acidification of only 5% of the total reactive ^{10}Be pool, showing that this pool is not resolvably affected by the relative short-term anthropogenic acidification. The measured $[^{10}Be]_{reac}$ thus likely reflects the erosion rate over the time scale of regolith weathering. We conclude that steady state between depositional and exported ^{10}Be fluxes is not given in Lysina today due to the high dissolved ^{10}Be export, but in pre-industrial times steady state would have been attained.

8. Stable ^{9}Be in parent bedrock and its release during weathering

8.1 Catchment-wide ^{9}Be concentrations in parent bedrock

Calculating meaningful denudation rates depends on representative estimates of ^{9}Be concentrations in the parent bedrock, $[^{9}Be]_{parent}$ (von Blanckenburg et al., 2012). Unlike in large watersheds (e.g. Wittmann et al., 2015, in the Amazon basin), assuming a mean upper continental crust value of 2.5 µg g^{-1} for $[^{9}Be]_{parent}$ (Rudnick and Gao, 2004) for small watersheds underlain by heterogeneous lithologies is not appropriate. Indeed, in particular in the mafic and ultramafic catchments we find highly variable rock types in the drill cores (Table S2), and all three lithologies feature high heterogeneity in [^{9}Be] of bedrock samples (Table 5, Figure 5). $[^{9}Be]_{bedrock}$ values range from 2.83 to 20.3 µg g^{-1} in the Lysina granite, from 0.43 to 2.89 µg g^{-1} for various mafic rock types present in Na Zeleném and range from <0.01 to 0.73 µg g^{-1} ^{9}Be in the ultramafic rocks of Pluhův Bor. The means of these ^{9}Be concentrations for the different parent bedrock types are comparable to published values of mafic and ultramafic rocks (Table 10). The high heterogeneity in [^{9}Be] for the Lysina granite is also found by other studies in the Czech Republic (Navrátil, 2000; Navrátil et al., 2002).

Because of this heterogeneity, simply averaging concentrations from a number of bedrock samples is unlikely to yield a representative parent concentration, and will in

any case be subject to a high uncertainty. We have thus developed two alternative approaches. The first is to compute a representative $[^9Be]_{parent}$ from the surface areal distribution of the different lithologies and their respective $[^9Be]_{bedrock}$. For Lysina this is simple. As the catchment features a granitic mono-lithology (medium-grained to porphyric granite) (Table S2), we can use the mean Be concentration presented in Table 5 as catchment-averaged value, assuming that this (although highly imprecise, due to very variable $[^9Be]_{bedrock}$) ^9Be concentration is distributed evenly throughout the catchment. Thus for the granite, the catchment-wide $[^9Be]_{parent}$ is identical to the average of all bedrock samples and is 5.4±4.8 µg g^{-1} (Table 5). For the Pluhův Bor catchment, the areal distribution of the bedrock has been assessed from point counting of bedrock outcrops (Krám et al., 2009), thereby providing an estimate of the surface areal distribution of bedrock types. The bedrock composition is composed of 51% serpentinite, 28% tremolite (schist) and actinolite (schist), 13% amphibolite and 8% other rocks. Weighing these rock type percentages with the corresponding $[^9Be]_{bedrock}$ from Table S2 yields a $[^9Be]_{parent}$ of 0.15 µg g^{-1} for the ultramafic Pluhův Bor catchment (Table 5). For the mafic Na Zeleném catchment spatially representative parent bedrock occurrences have not been mapped.

Therefore, in a second approach we use the averaging nature of river sediment to estimate spatially representative $[^9Be]_{parent}$. However, it is important to note that the mobilisation of soluble elements, such as Na, Ca, Mg, and Si induces sometimes significant mass loss during weathering, such that the sum of $[^9Be]_{reac}$ and $[^9Be]_{min}$ does *not* reflect the parent concentration $[^9Be]_{parent}$, even if no Be was lost in the dissolved form. Thus, we first identify an element in river sediment ($[X]_{bedload\text{-}sediment}$) that has not been affected by any loss or river-bed particle sorting when compared to bedrock concentrations ($[X]_{bedrock}$). We do this by plotting averaged $[X]_{bedrock}$ versus $[X]_{bedload\text{-}sediment}$ (Fig. 7). For an element that plots on the 1:1 line, $[X]_{bedload\text{-}sediment}$ provides a representative bedrock concentration. For the Lysina catchment, this approach directly yields a good coincidence for the catchment-wide $[^9Be]_{bedload\text{-}sediment}$ which yields 5.5 µg g^{-1} as compared to 5.4 µg g^{-1} for the average $[^9Be]_{bedrock}$ (Fig. 7A).

In the mafic and ultramafic catchments $[^9Be]_{bedload\text{-}sediment}$ is much higher than $[^9Be]_{bedrock}$ (Table 5) due to mass loss of major elements during weathering. We thus need to identify the representative $[^9Be]_{parent}$ from multiple $[^9Be]_{bedrock}$ values. We identified from Fig. 7 major elements of which $[X]_{bedload\text{-}sediment}$ plots on the 1:1 line and that are thus representative for the catchment-wide bedrock concentration. We then plotted for each of these representative elements their $[X]_{bedrock}$ measured in individual bedrock samples against $[^9Be]_{bedrock}$ of the same samples (Fig. 8). If $[X]_{bedrock}$ correlates reasonably well

with Be, the representative $[^{9}Be]_{parent}$ can be calculated from the intersection of the major element's bedload sediment concentration with the slope of the linear trend. We chose the elements K for Na Zeleném and Al for Pluhův Bor. Applying this linear regression for Na Zeleném, a $[^{9}Be]_{parent}$ of 1.21 µg g^{-1} is derived, and for Pluhův Bor a $[^{9}Be]_{parent}$ of 0.18 µg g^{-1} results (Fig. 8). For Pluhův Bor this $[^{9}Be]_{parent}$ compares well to the rock type-weighed $[^{9}Be]_{parent}$ determined on the bedrock core samples which is 0.15 µg g^{-1} (Table 5). We thus use these catchment-wide $[^{9}Be]_{parent}$ values (summarized in Table 5) to calculate denudation rates.

8.2 Mobilized ^{9}Be fraction and ^{9}Be fluxes

The fraction of ^{9}Be that is mobilized from primary minerals during weathering termed $\left(\boldsymbol{f}_{\boldsymbol{reac}}^{\boldsymbol{9Be}} + \boldsymbol{f}_{\boldsymbol{diss}}^{\boldsymbol{9Be}}\right)_{min/reac}$ is a parameter required to calculate denudation rates and can be determined from eq. 3. However, like $[^{10}Be]_{reac}$ (section 7.2), the ratio $\frac{[\,^{9}\mathrm{Be}]_{\mathrm{min}}}{[\,^{9}\mathrm{Be}]_{\mathrm{reac}}}$ used in this calculation might be biased in river sediment from particle sorting. Note that in this case this bias is propagated into the derived denudation rates (eq. 2, Table 12). This grain size dependence becomes apparent when we compare the estimate using $[^{9}Be]_{reac}$ and $[^{9}Be]_{min}$ from the <63 µm grain size fraction with that from the 125 µm fraction (Table 2). We argue that the "bulk" estimate gives a reasonable estimate of the mobilized fraction of ^{9}Be. These $\left(\boldsymbol{f}_{\boldsymbol{reac}}^{\boldsymbol{9Be}} + \boldsymbol{f}_{\boldsymbol{diss}}^{\boldsymbol{9Be}}\right)_{min/reac}$ are 0.1 for Lysina, 0.5 for Na Zeleném and 0.37 for Pluhův Bor (Table 11). If the Be mobilization from primary minerals is interpreted as a proxy for the degree of weathering of the bulk rock, this comparison indicates a much higher degree of weathering in the mafic and ultramafic catchments than in the granitic Lysina catchment.

Relative higher degrees of weathering are expected for mafic and ultramafic lithologies, which contain a higher amount of easily weatherable minerals, such as amphibole, plagioclase, or serpentine minerals. These will also be the carriers of Be. In the granite, in contrast, quartz, K-feldspar, and muscovite are slow to weather. In addition, the high variability of $[^{9}Be]_{bedrock}$ in the granite, the good agreement between average $[^{9}Be]$ in bedrock and that in river sediment, and the unusually high $[^{9}Be]_{parent}$ of 5.5 µg g^{-1} lets us suspect that an important carrier of Be_{min} in the granite are accessory Be-rich minerals, such as beryl and phenakite that are extremely resistant to weathering.

9. Erosion and denudation rates

9.1 Erosion rates from meteoric $[^{10}Be]_{reac}$

Erosion rates E_{met} were calculated from $[^{10}Be]_{reac}$ using eq. 1 with a depositional flux of 1.46×10^6 ats ^{10}Be cm^{-2} y^{-1} and the measured parameters listed in Table 12 for the "bulk" grain size fraction. Erosion rate estimates further require a correction for the loss of ^{10}Be in the dissolved form (q/K_d term in eq. 1a). This correction is most relevant if the K_d is low and runoff q is high (see Appendix A in von Blanckenburg et al., 2012). We have seen in section 6.1 that the largest dissolved loss occurs in the granitic Lysina catchment, due to its low pH. Employing the loss correction (eq. 1a), and using an estimated pre-industrial pH of 5.5 (Table 8), we get E_{met} of 225 ± 24 t km^{-2} y^{-1} (Table 12). In the mafic and ultramafic catchments, dissolved ^{10}Be loss is negligible due to the neutral pH and thus the effect of the correction is smaller than the derived uncertainties. E_{met} denote to 50.2 ± 5.3 t km^{-2} y^{-1} for the mafic Na Zeleném and 64.4 ± 7.0 t km^{-2} y^{-1} for ultramafic Pluhův Bor catchments, respectively (Table 12).

These erosion rates, being among the first ever measured with cosmogenic nuclides in mafic and ultramafic catchments and integrating over the weathering time scale (10^4 kys), are higher than erosion rates from 10^1 y sediment yield data for catchments in the Czech Republic that range from 8 to 32 t km^{-2} y^{-1} (Vanmaercke et al., 2011). These estimates are from river load gauging or from reservoir siltation rates. In small catchments gauging-derived estimates commonly miss out on the low-frequency high-magnitude sediment transport events, due to the much shorter integration time scales than cosmogenic nuclide methods, a phenomenon commonly observed in Middle European upland catchments (Schaller et al., 2001; Meyer et al., 2010) (see Section 9.2.1).

9.2 Denudation rates from ^{10}Be(meteoric)/^{9}Be ratios

Denudation rates D_{met} were calculated using eq. 2, $(^{10}Be/^{9}Be)_{reac}$ from Table 3, $[^{9}Be]_{parent}$ from Table 5, and $(f^{9}_{reac}+f^{9}_{diss})$ from Table 11. Sorting might affect denudation rates as $\left(\boldsymbol{f^{9Be}_{reac}} + \boldsymbol{f^{9Be}_{diss}}\right)_{min/reac}$ (eq. 3) depends on grain size. Here, we rely on our "bulk" grain size estimation. Low Be retentivity will affect denudation rates to a smaller degree than erosion rates (eq. 2a). Differences in D_{met} due to retentivity that are outside of uncertainties only emerge for the acidic Lysina catchment. Depending on K_d scenario used, D_{met} is between 203 ± 25 (no correction) and 185 ± 23 t km^{-2} y^{-1} (correction with pre-industrial pH). For the mafic Na Zeleném catchment D_{met} is 112 ± 14 t km^{-2} y^{-1}, and for the ultramafic Pluhův Bor catchment 153 ± 19 t km^{-2} y^{-1} (Table 12). These

uncertainties do not include a potentially systematic error from using spatially non-representative $[^9Be]_{parent}$; an overestimation of $[^9Be]_{parent}$ would result in an underestimation of D_{met}. For example, when using the median $[^9Be]_{parent}$ of 3.5 µg g^{-1} for Lysina instead of a spatially-averaged value of 5.5 µg g^{-1} (Table 5), the resulting D_{met} would increase to 312 t km^{-2} y^{-1}.

These denudation rates have integration time scales of 24.5 kys for Lysina (using the inventory approach) and 20-21 kys for for Na Zeleném and Pluhův Bor using soil depths as estimate for ^{10}Be percolation depths (section 7.1).

9.2.1 Comparison to independent estimates of weathering

We can estimate weathering from comparing E_{met} to D_{met}, as the remainder should comprise a weathering rate. When comparing E_{met} to D_{met}, we note that in case of Lysina, E_{met} (225 t km^{-2} y^{-1}) is higher than the D_{met} (185 t km^{-2} y^{-1}), just beyond limits of uncertainty. E being higher than D should be impossible given that D includes a weathering component in addition to E. Thus, we suggest that E_{met} being higher than D_{met} in Lysina is an artifact arising from using a bulk grain size that is too coarse, and thus related bulk-$[^{10}Be]_{reac}$ is too low, or from using $[^9Be]_{parent}$ that is too high, and hence D_{met} is too low. In the other catchments, E_{met} comprises a fraction of ~0.5 of D_{met}, which is roughly concurrent with estimated CDF´s for catchments of similar climate, vegetation, drainage area, tectonic parameters (such as relief), but not lithology. These CDF's were measured in granitic lithologies (Dixon and von Blanckenburg, 2012). W/E estimates from mafic rock are still barely existing. However, a similar high degree of gross weathering (meaning release from primary minerals) is also indicated by $\left(f_{reac}^{9Be} + f_{diss}^{9Be}\right)_{min/reac}$ (Section 8.2) that are around 0.4-0.5 for the (ultra-)mafic catchments of Na Zeleném and Pluhův Bor (Table 11).

Other estimates of the weathering flux (comprising dissolved flux after precipitation of secondary minerals) are much lower than these estimates. For example, Krám et al. (2012), by using the *MAGIC* model, derived net chemical weathering rates of 1.3 to 3.4 t km^{-2} y^{-1} from Mg, Ca, K, and Na concentrations (excluding the SiO_2 component) for the studied catchments. We derive similar chemical weathering rates by using silicate-derived total dissolved solids (of all base cations, i.e. Mg, Ca, K, Na, and SiO_2, all corrected for atmospheric input using element/Cl ratios and using the precipitation record of the Lysina catchment; Krám et al. (2012) and discharge data from all three catchments (Table S7). These chemical weathering rates are about 6 t km^{-2} y^{-1} for the felsic Lysina, 8 t km^{-2} y^{-1} for the mafic Na Zeleném, and 10 t km^{-2} y^{-1} for the ultramafic Pluhův Bor catchment. These rates are in the order of other published chemical

weathering rates from adjacent areas. For example, Pačes (1986) found chemical weathering rates of 4 to 6 t km^{-2} y^{-1} for small forested upland catchments that are underlain by gneiss in the Bohemian Massif, and Oliva et al. (2003) and Schaller et al. (2001) obtained chemical weathering rates for small granitic catchments in Europe ranging from 3 to 10 t km^{-2} y^{-1}.

Reconciling these low weathering rates with high denudation/erosion rates from meteoric cosmogenic nuclides is subject to substantial speculation. Such a deficit in fluxes from dissolved river loads relative to those from cosmogenic nuclides, however, is a ubiquitous observation in Middle European upland catchments (Schaller et al, 2001). One potential explanation lies in the different time scales that these methods integrate over. Dissolved loads usually integrate over a few decades only, whereas meteoric denudation and weathering rates integrate over the entire Holocene and even to before the LGM, resulting in possible non-steady state of fluxes (section 7). A full analysis of the reasons of this phenomenon is beyond the scope of this paper.

9.3 Comparison of meteoric-derived to *in situ*-derived denudation rates

In situ-derived denudation rates from ^{10}Be in quartz in river sediment are an established tool (e.g. von Blanckenburg, 2005; Granger and Schaller (2014)) that we compare our meteoric-derived denudation rates with (Fig. 9). D_{met} (Table 12) and D_{insitu} (Table 7) agree within uncertainty for the mafic Na Zeleném catchment (Fig. 9), and differ by about 45% for the felsic Lysina catchment. For the ultramafic Pluhův Bor catchment, D_{insitu} (46 t km^{-2} y^{-1}) and D_{met} (153 t km^{-2} y^{-1}) differ by a factor of 3. In this catchment, quartz occurs in veins that are intersecting the bedrock. These veins are commonly formed during alteration of peridotite to antigorite when serpentinite forms and the subsequent release of SiO_2 is re-precipitated as joint fillings (Cleaves et al., 1974). These quartz veins would potentially erode slower than the surrounding bedrock and thus could exhibit higher *in situ* cosmogenic nuclide concentrations (Codilean et al., 2014). We suggest that the low D_{insitu} in this catchment is thus due to a lithological bias.

The determined D_{insitu} (Table 7) of the granitic and mafic catchment are in the range of *in situ* cosmogenic denudation rates for (granitic) upland catchments of middle Europe (Schaller et al. (2001). Schaller et al. (2001) measured *in situ* ^{10}Be denudation rates in river catchments with vegetation cover and precipitation rates similar to our catchments. For example, the crystalline Regen catchment, although being larger than our catchments, exhibits denudation rates of 65 to 104 t km^{-2} y^{-1}, thereby integrating over time scales of 10 to 40 ky (recalculated in Schaller et al. (2002b)).

10. Conclusions

We have provided an extensive field test of the new $^{10}Be(meteoric)/^{9}Be$ method that is suited to determine denudation rates, erosion rates, and the degree of weathering for sediment from catchments draining mafic and ultramafic rock. We have also extensively tested the assumptions this method is based on, and evaluated requirements for the successful application of the new proxy. The main results of these tests are:

- The sedimentary and dissolved ^{10}Be export fluxes are balanced with atmospheric deposition fluxes to within the 50% uncertainty of the estimates which means that ^{10}Be flux global distribution maps can be used with sufficient confidence.
- ^{10}Be and ^{9}Be concentrations from the reactive phase strongly depend on grain size, but the $(^{10}Be/^{9}Be)_{reac}$ ratio is independent of grain size. Because ^{10}Be concentrations are used to estimate erosion rates and the mobile fraction of ^{9}Be is needed to calculate denudation rates, the need exists to map out a grain size range for which these parameters are insensitive to grain size.
- The $^{10}Be/^{9}Be$ ratio in dissolved Be equilibrates preferably with the amorphous oxide phase, indicating that the isotope ratio from both “reactive” Be attached to sediment and dissolved Be can be used to calculate denudation rates.
- Under acidic environmental conditions, a correction for the dissolved ^{10}Be loss is required, especially in those affected by acid rain. This loss is negligible in mafic and ultramafic rock due to pH buffering. Comparing the total reactive pool of ^{10}Be to what is lost to the dissolved phase since anthropogenic acidification however leads us to assume that the reactive pool integrating over the weathering time scale is not affected by this loss.
- Determining the parent ^{9}Be concentration, required as an input to calculate denudation rates, is difficult in small catchments due to parent rock heterogeneity. We suggest an approach by a multi-element regression comparing bedload and bedrock elemental and ^{9}Be data to estimate a representative, catchment-wide $^{9}Be_{parent}$ concentration.
- Analyses of ^{10}Be depth profiles in drill cores shows ^{10}Be penetration that exceeds 4 m depth. Thus the surface nuclide concentrations are not excessively sensitive to perturbation such as those resulting from material translocation during the transition from the last cold stage into the Holocene.

The here presented first-ever results of cosmogenic denudation rates for non-felsic lithologies that agree with *in situ*-derived denudation rates to within 50% are encouraging. Specifically, denudation rates D_{met} from $^{10}Be/^{9}Be$ for small upland European catchments are 185 t km^{-2} y^{-1} in the granitic, 112 t km^{-2} y^{-1} in the mafic and 153 t km^{-2} y^{-1} in the ultramafic catchment, whereas denudation rates D_{insitu} derived from *in situ* cosmogenic ^{10}Be in quartz on sand-sized bedload sediment yield 101 t km^{-2} y^{-1} in the granitic and 91 t km^{-2} y^{-1} in the mafic catchment, respectively. Only in the ultramafic catchment, where quartz is present in veins potentially eroding slower, D_{insitu} is with 46 t km^{-2} y^{-1} lower than D_{met}. Further, derived degrees of weathering indicated from the flux of ^{9}Be liberated by dissolution from primary minerals is ca. 0.4 to 0.5 which is common for these supply-limited settings and mafic/ultramafic lithologies. Hence, the $^{10}Be/^{9}Be$ approach can now be used to explore erosion, weathering, and denudation of, for example, basaltic and andesitic rocks to determine these rates in volcanic island settings that have been proposed to substantially contribute to the global weathering and erosion budget.

Acknowledgements

We thank the Helmholtz Association and the *SoilTrEC* project for support. We also thank R. Naumann and A. Gottsche for performing XRF and XRD analysis, H. Rothe, H. Schopka and J. Bouchez for help with performing HR-ICP-MS analysis. We are especially indebted to J. Schuessler for help during several sampling campaigns and V. Štědrá and T. Jarchovský for petrological descriptions of borehole drill cores. We thank two anonymous reviewers for useful comments.

Figures and captions

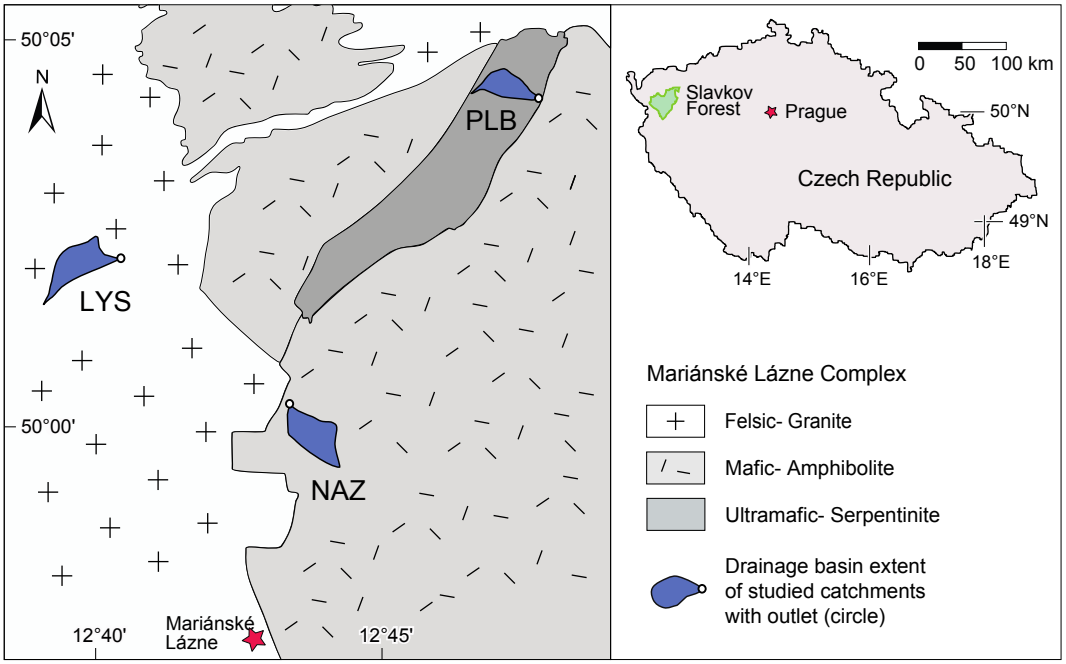

Figure 1: Small map: Slavkov Forest area (in green) in the NW of the Czech Republic. Large map: Simplified map of the Mariánské Lázně Complex (modified after Jelínek and Štědrá (1997)). Catchments shown not to scale; LYS = Lysina (felsic), NAZ = Na Zeleném (mafic), and PLB = Pluhův Bor (ultramafic).

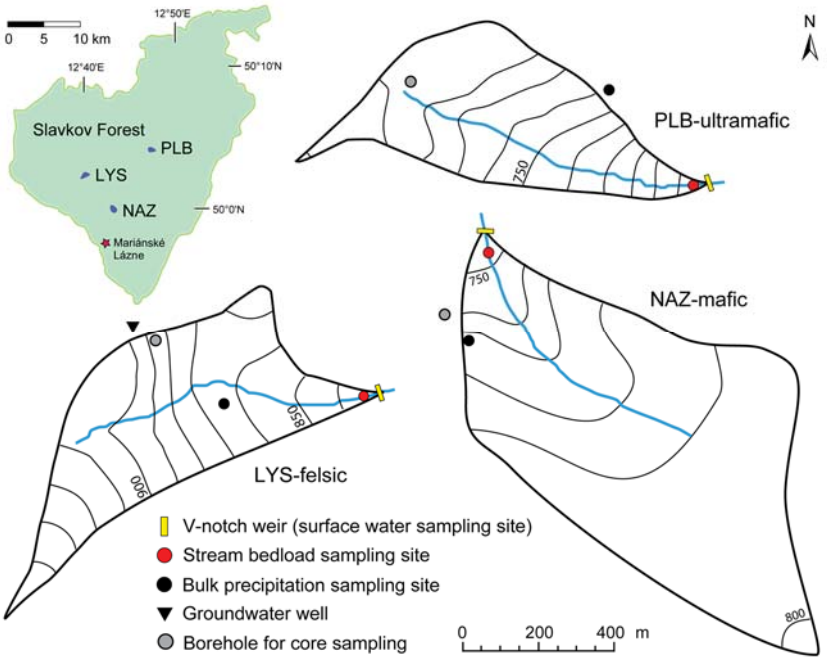

Figure 2: Detailed drainage areas of each catchment with 10 m elevation contours and sampling sites. Catchments drawn at arbitrary geographic positions. Inset map shows the location of the catchments within the Slavkov Forest. LYS = Lysina, NAZ = Na Zeleném, PLB = Pluhův Bor.

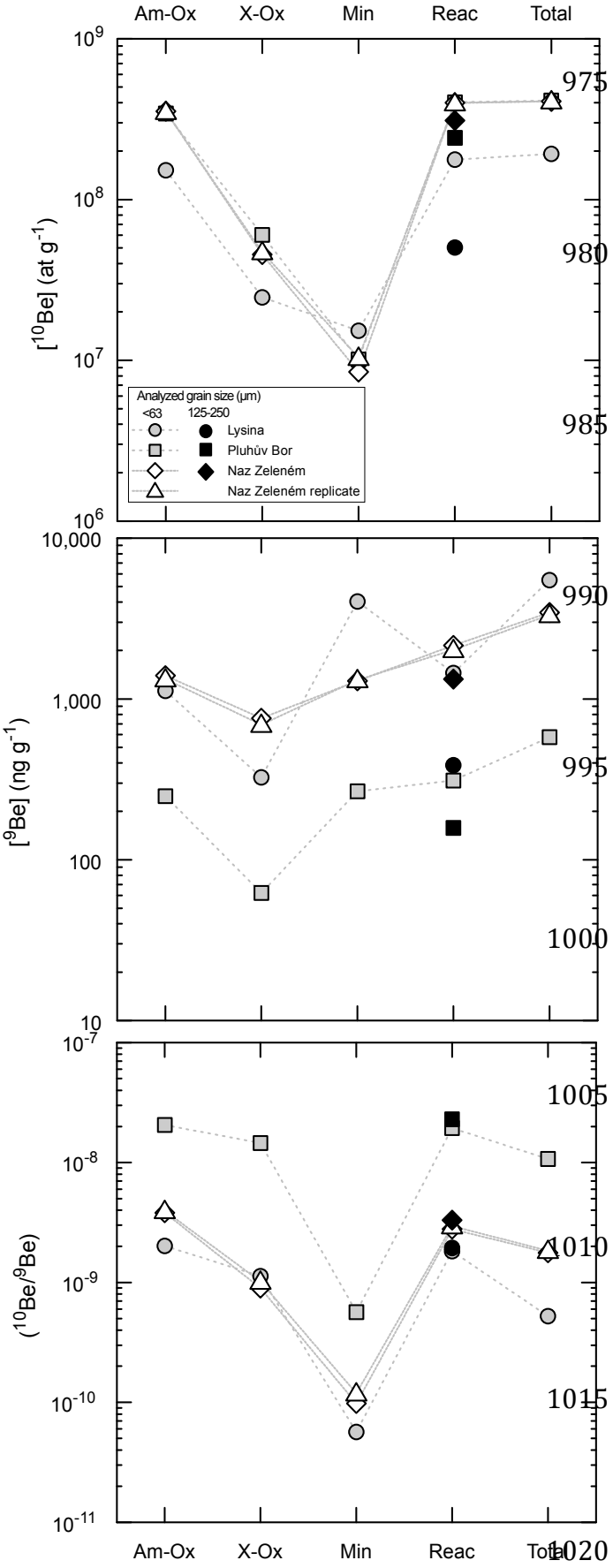

Figure 3, A: Concentrations of ^{10}Be (in ats g^{-1}) **B:** ^{9}Be (in ng g^{-1}) and **C:** resulting $^{10}Be/^{9}Be$ ratios for the sequentially extracted fractions for the <63 µm grain size fraction and the 125-250 µm grain size fraction (measured on "reac" fraction only). Measured extracted fractions are "am-ox" (amorphous oxides) and "x-ox" (crystalline oxides), whereas "min" is silicate residual. Note that "reac" is calculated (except for 125-250 µm grain size fraction) as the summed reactive fraction (am-ox + x-ox) and "total" is the sum of all measured Be concentrations (am-ox + x-ox + min). Displayed symbols are larger than uncertainties. LYS = Lysina (felsic), NAZ = Na Zeleném (mafic), PLB = Pluhův Bor (ultramafic).

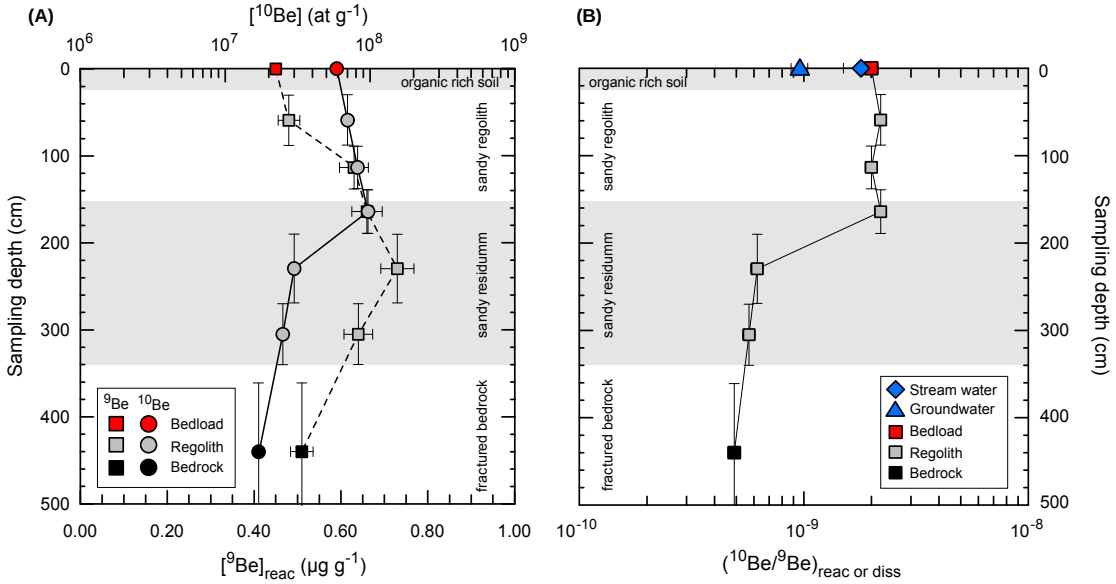

Figure 4: Results from the drilled core at Lysina (granitic catchment). All measurements were performed on bulk samples sieved to <2 mm. **A:** $[^{10}Be]_{reac}$ (upper x-axis; circles) and $[^{9}Be]_{reac}$ (lower x-axis; squares) and **B:** $(^{10}Be/^{9}Be)_{reac}$. Vertical bars display the uncertainty in depth derived from sampling. Note that the deepest sample at a depth of 4.4 m represents a highly weathered fragment of fractured bedrock. For comparison we show the $[^{10}Be]_{reac}$ and $[^{9}Be]_{reac}$ and $(^{10}Be/^{9}Be)_{reac}$ determined on bulk bedload (<500 µm) (Table 3), $(^{10}Be/^{9}Be)_{diss}$ measured in stream water, and $(^{10}Be/^{9}Be)_{diss}$ measured in groundwater, respectively. Note that dissolved $[^{10}Be]$ (~10^4 ats g^{-1}) and $[^{9}Be]$ (ng L^{-1}) are not shown as they are much lower than $[^{9 \text{ or } 10}Be]_{reac}$.

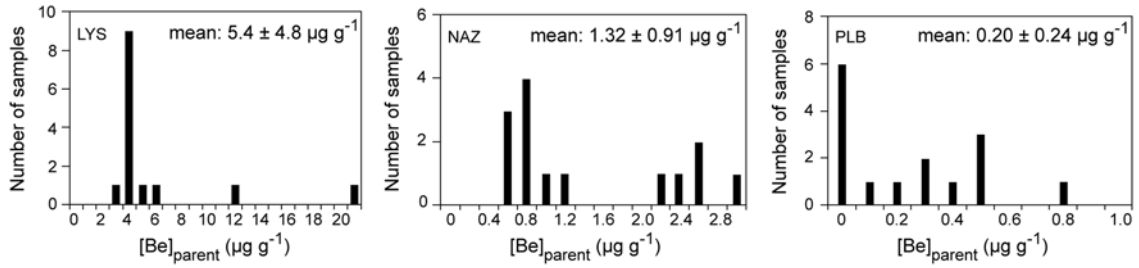

Figure 5: Histograms showing the distribution of [Be] in bedrock core samples (in µg g^{-1}, Table S2) in the individual catchments. Mean Be concentration is given ± 1SD (in µg g^{-1}). LYS = Lysina (felsic), NAZ = Na Zeleném (mafic), PLB = Pluhův Bor (ultramafic).

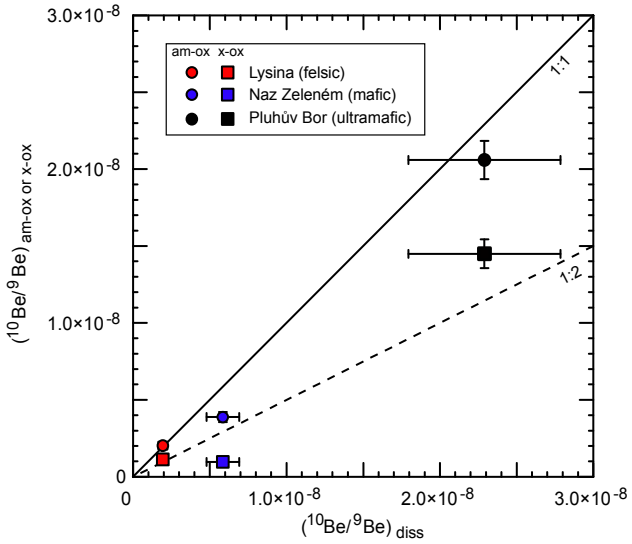

Figure 6: Reactive $^{10}Be/^{9}Be$ ratios determined on the am-ox and x-ox fractions versus dissolved $^{10}Be/^{9}Be$ stream water ratios sampled simultaneously (Aug. 2011). Propagated analytical uncertainties of ^{9}Be and ^{10}Be measurements (Table S5) are shown.

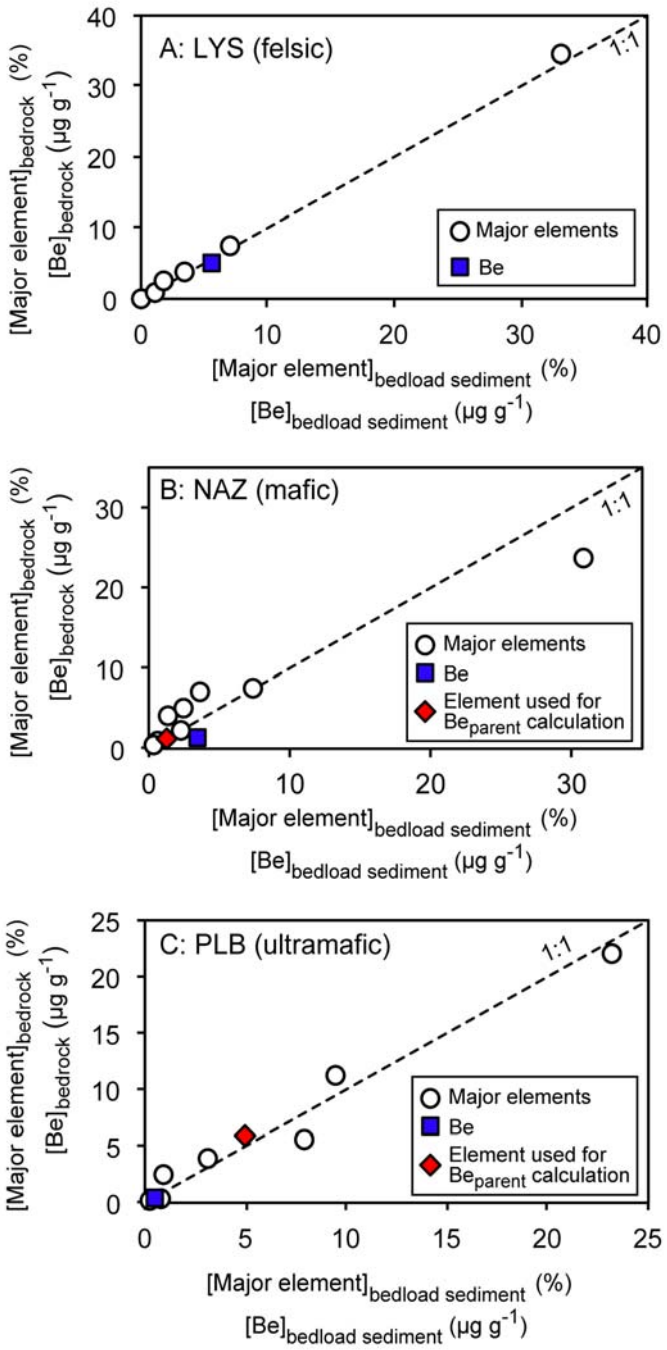

Figure 7: Average Be concentrations (Table S2) and average concentrations of major elements (Si, Ti, Al, Fe, Mn, Mg, Ca, Na, K, Table S3) of bedrock, plotted versus major elemental (Table S4) and Be concentrations (Table 2) determined in bedload sediment of each catchment. [Major element] (in %) were measured with XRF (white circles), and [Be] (in µg g^{-1}) with ICP-OES (blue squares). In case of NAZ and PLB, red symbols show the element chosen for calculation of $[^{9}Be]_{parent}$ (being K for NAZ and Al for PLB, see Fig. 8). Stippled line is the 1:1 line. LYS = Lysina (felsic), NAZ = Na Zeleném (mafic), PLB = Pluhův Bor (ultramafic).

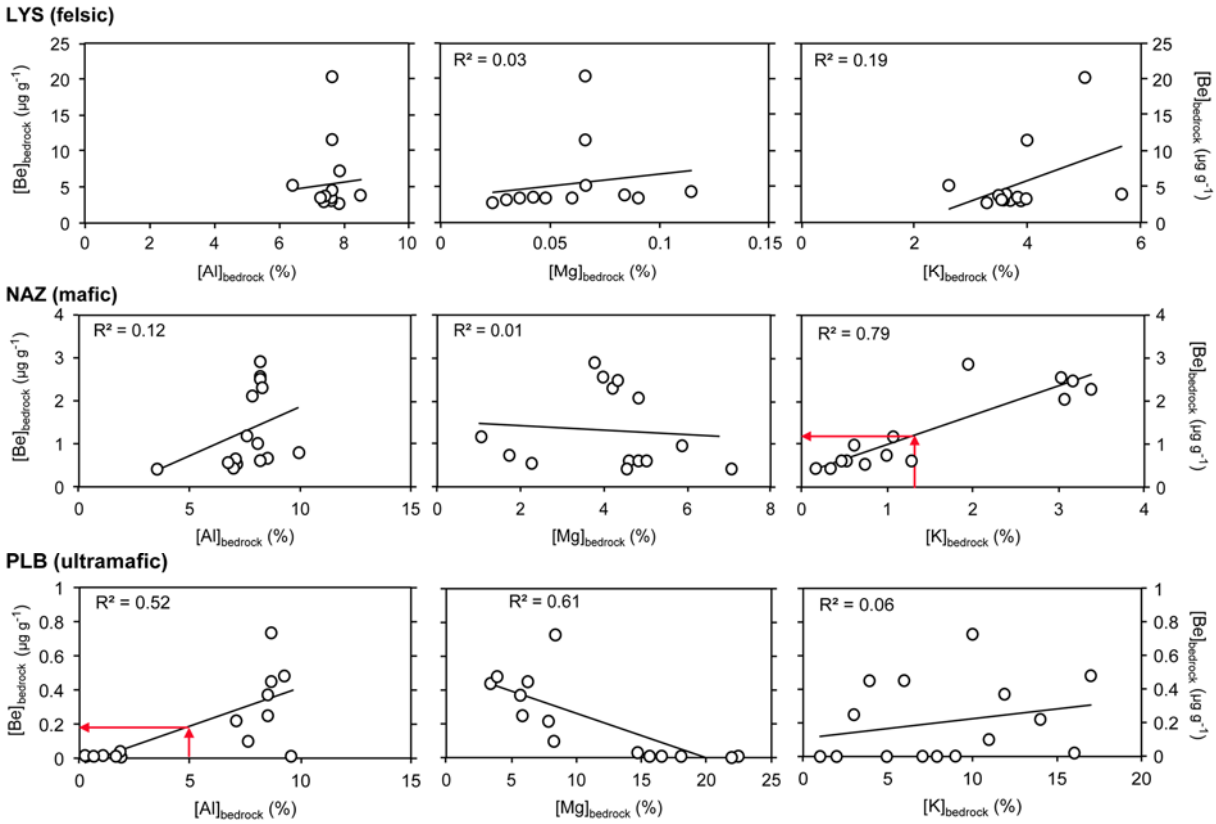

Figure 8: Linear regression used in section 8.1 to estimate a catchment-wide averaged $[^9Be]_{parent}$. $[^9Be]_{bedrock}$ measured in bedrock core samples (Table S2) are plotted versus major element $[X]_{bedrock}$ (Al, Mg, and K) concentrations measured in the same bedrock samples (Table S3). The black line is the linear fit line through all individual data points (open circles). Red arrows show how a $[^9Be]_{parent}$ is derived from the bedload sediment concentration of K (1.3 %) at NAZ and Al (5.0 %) at PLB, respectively, which are the only elements that correlate reasonably well with Be. Note that although Mg also correlates with Be in the case of PLB, it is not used here as it is likely underestimated in bedload sediment because it is lost into the dissolved fraction (Fig. 7). The overall poor correlation in the (ultra)mafic catchments is likely due to the chemically highly heterogeneous bedrock types.

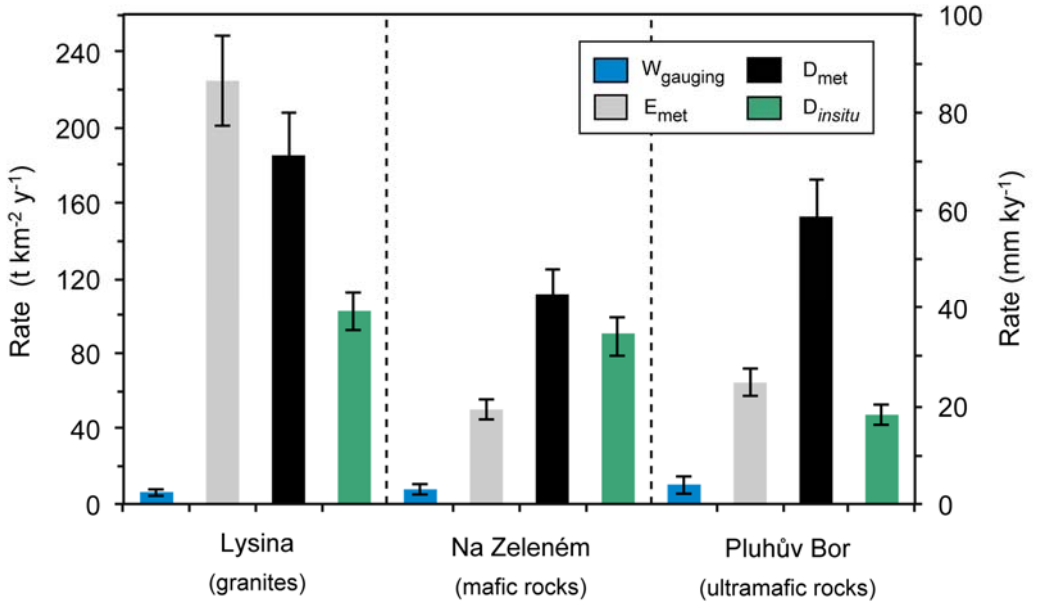

Figure 9: Summary of Earth surface fluxes determined in this study. Chemical weathering fluxes derived from gauging data ($W_{gauging}$, in blue, section 9.2.1), erosion rates calculated from meteoric ^{10}Be (E_{met}, in grey, Table 12, using bulk estimates and a K_d read from linear trend line), denudation rates calculated from ^{10}Be(meteoric)/^{9}Be ratios (D_{met}, in black, Table 12), and *in situ*-derived denudation rates (D_{insitu}, in green, Table 7, using bulk estimates and a K_d read from linear trend line) for all three catchments in t km^{-2} y^{-1} and mm ky^{-1}.

Tables

Table 1: Location and characteristics of the three studied catchments in the Slavkov Forest, Czech Republic.

Catchment	Lysina (LYS)	Na Zeleném (NAZ)	Pluhův Bor (PLB)
Coordinates of catchment outlet	50°2.069'N, 12°40.149'E	49°59.896'N, 12°42.563'E	50°3.389'N, 12°47.309'E
Drainage area (km^2)	0.273	0.55	0.216
Altitude range and mean (m.a.s.l.)	829 - 949 (881)	736 - 802 (793)	690 - 804 (765)
Slope (%)	11.5	5	13
Mean discharge (L s^{-1}) [1]	3.0	5.5	1.1
Stream water pH	4.2	6.9	7.6
Underlying bedrock	felsic (granite)	mafic (amphibolite)	ultramafic (serpentinite, amphibolite)
Mineral composition[2]	quartz, plagioclase, muskovite, illite, orthoclase, kaolinite	hornblende, plagioclase, quartz, muscovite, chlorite, rutile, magnetite	hornblende, quartz (veins), serpentine, talc, chlorite, plagioclase, vermiculite, magnesite
Soil type	Podzol, Gleysol	Cambisol	Stagnosol
Mean soil depth (cm)	150	90	120
Vegetation cover	Norway spruce	Norway spruce	Norway spruce, Scots pine
Beginning of monitoring period	1989	2001	1991

Note that all three catchments form a CZO (Critical Zone Observatory) in the framework of the European Commission project *SoilTrEC* (Menon et al., 2014; Regelink et al., 2015).

[1] From Krám et al. (2012).

[2] Qualitative composition derived from X-ray diffraction (XRD) measurements (using a Bruker-axs D5000 Diffractometer) of fine-grained bedload (<63 µm) sediment. XRD results sorted from highest to lowest amount.

Table 2: Results of ^{9}Be and ^{10}Be concentrations and resulting ($^{10}Be/^{9}Be$) for bedload samples.

Sample ID	Grain size (µm)	Extracted fraction [1]	Initital solid sample weight (g)	[^{10}Be] [2] ($x10^{6}$ ats g^{-1})	[^{9}Be] [3] (ng g^{-1})	($^{10}Be/^{9}Be$) [2] ($x10^{-10}$)
Felsic Lysina catchment (Granite)						
LYS <63	**< 63**	**am-ox + x-ox**	**0.5069**	**176.5 ± 5.4**	**1449 ± 61**	**18.2 ± 1**
LYS <63	< 63	min	0.5069	15.31 ± 0.75	4040 ± 210	0.57 ± 0.04
LYS <63	< 63	total	0.5069			5.23 ± 0.26
LYS 63	63-125	reac	0.505		1067 ± 41	
LYS 125	**125-250**	**reac**	**0.7531**	**50.3 ± 1.6**	**387 ± 15**	**19.4 ± 1**
LYS 250	250-500	reac	1.0067		320 ± 13	
LYS "Bulk" [4]	< 500			58.7 ± 2.4	447 ± 10	
Mafic Na Zeleném catchment (Amphibolite)						
NAZ <63-1	**< 63**	**am-ox + x-ox**	**0.5092**	**400 ± 11**	**2154 ± 83**	**27.8 ± 1.3**
NAZ <63-1	< 63	min	0.5092	8.46 ± 0.46	1294 ± 67	0.98 ± 0.07
NAZ <63-1	< 63	total	0.5092			17.7 ± 0.74
NAZ <63-2	**< 63**	**am-ox + x-ox**	**0.522**	**398 ± 11**	**2020 ± 74**	**29.5 ± 1.4**
NAZ <63-2	< 63	min	0.522	10.43 ± 0.76	1312 ± 66	1.19 ± 0.11
NAZ <63-2	< 63	total	0.522			18.4 ± 0.76
NAZ 63	63-125	reac	0.5031		1696 ± 67	
NAZ 125	**125-250**	**reac**	**0.7533**	**310.4 ± 5.1**	**1403 ± 55**	**33.1 ± 1.4**
NAZ 250	250-500	reac	1.0043		1055 ± 42	
NAZ "Bulk" [4]	< 500			276 ± 10	1322 ± 28	
Ultramafic Pluhúv Bor catchment (Serpentinite)						
PLB <63	**< 63**	**am-ox + x-ox**	**0.5649**	**403 ± 11**	**311 ± 13**	**194 ± 10**
PLB <63	< 63	min	0.5649	10.12 ± 0.5	267 ± 14	5.66 ± 0.41
PLB <63	< 63	total	0.5649			107 ± 4.6
PLB 63	63-125	reac	0.7552		216.7 ± 9.3	
PLB 125	**125-250**	**reac**	**1.0059**	**242.1 ± 4.4**	**157.8 ± 6.8**	**230 ± 11**
PLB 250	250-500	reac	1.0256		141.5 ± 6	
PLB "Bulk" [4]	< 500			225 ± 10	157.4 ± 4.3	

[1] "am-ox + x-ox": both phases measured separately for ^{10}Be and ^{9}Be concentrations (see supplement for extraction-specific data); "reac": am-ox and x-ox were extracted separately but then combined to one "reac" phase for AMS measurement; "min" = mineral-residual after chemical extraction; "total"= reac + min.

Bold: Different grain size or replicate samples where $^{10}Be/^{9}Be$ data was obtained for the reac fraction.

[2] ^{10}Be concentrations were only determined for <63 µm and 125-250 µm grain size fractions (all other values were calculated in Table 3) combined analytical and blank error (all uncertainties 1σ) is given.

[3] Uncertainty given comprises a 5% ICP-OES uncertainty that was propagated through all calculations.

[4] All concentrations were calculated by weighting the [Be] with the mass of the respective grain size fraction. For details, see Table 3.

Table 3: Deriving reactive ^{10}Be and ^{9}Be concentrations for "bulk" (<500 µm) samples.

Sample ID	Grain Size (µm)	Fractional amount of grain size (rel. to total)	Measured total ^{10}Be concentration [1] ($x10^6$ ats g^{-1})	Reactive ^{9}Be concentration (ng g^{-1})	$(^{10}Be/^{9}Be)_{reac}$	Recalculated total ^{10}Be concentration ($x10^6$ ats g^{-1})
Felsic Lysina catchment (Granites)						
LYS	< 63	0.05	191.9 ± 5.4	1449 ± 61	19.82 ± 1	190 ± 14
LYS 63	63-125	0.07		1067 ± 41		140 ± 10
LYS 125	125-250	0.21	50.3 ± 1.6	387 ± 15	19.44 ± 0.98	50.8 ± 3.6
LYS 250	250-500	0.66		320 ± 13		42 ± 3
LYS Average [2]					19.6 ± 1.4	
LYS "Bulk" [3]	**< 500**			**447 ± 10**		**58.2 ± 2.4**
Mafic Na Zeleném catchment (Amphibolite)						
NAZ	< 63	0.1	409 ± 11	2087 ± 80	29.3 ± 1.4	435 ± 28
NAZ 63	63-125	0.12		1696 ± 67		354 ± 23
NAZ 125	125-250	0.25	310.4 ± 5.1	1403 ± 55	33.1 ± 1.4	293 ± 19
NAZ 250	250-500	0.53		1055 ± 42		220 ± 14
NAZ Average Ratio [2]					31.2 ± 2	
NAZ "Bulk" [3]	**< 500**			**1322 ± 28**		**276 ± 10**
Ultramafic Pluhúv Bor catchment (Serpentinite)						
PLB	< 63	0.04	413 ± 11	311 ± 13	199 ± 10	446 ± 31
PLB 63	63-125	0.07		216.7 ± 9.3		310 ± 21
PLB 125	125-250	0.23	242.1 ± 4.4	157.8 ± 6.8	230 ± 11	226 ± 16
PLB 250	250-500	0.66		141.5 ± 6		203 ± 14
PLB Average Ratio [2]					214 ± 15	
PLB "Bulk" [3]	**< 500**			**157.4 ± 4.3**		**225 ± 10**

[1] Total (reac + min) used for ^{10}Be as entire ^{10}Be reservoir is needed for calculating the ^{10}Be inventory.

[2] Averaged $(^{10}Be/^{9}Be)_{reac}$ ratio used for recalculation of $[^{10}Be]_{bulk}$ and $[^{9}Be]_{bulk}$.

[3] All concentrations were calculated by weighting the [Be] with the mass of the respective grain size fraction.

Table 4: $[^{9}Be]_{reac}$, $[^{10}Be]_{reac}$, $(^{10}Be/^{9}Be)_{reac}$ and resulting ^{10}Be inventory for the core taken at Lysina (granitic).

	Sample description	Sampling depth [1] (cm)	Integrated depth (from drilling case) (cm)	Depth interval used for inventory calculation (cm)	Initial sample weight (g)	$[^{10}Be]_{reac}$ [2] ($x10^6$ ats g^{-1})	$[^{9}Be]_{reac}$ [2] (ng g^{-1})	$(^{10}Be/^{9}Be)_{reac}$ [2] ($x10^{-10}$)	^{10}Be Inventory [3] ($x10^8$ ats cm^{-2})
LYS C	sandy soil	60	30-88	57.5	0.7577	70.3 ± 2.3	484 ± 25	21.7 ± 1.3	72.7
LYS 1	sandy soil	115	89-138	50.0	0.7503	82.3 ± 2.7	630 ± 33	19.6 ± 1.2	74.1
LYS 2	sandy residuum	160	139-189	51.5	0.7525	97 ± 3.2	664 ± 35	21.8 ± 1.3	89.9
LYS 4	sandy residuum	218	190-269	80.0	0.7562	30.2 ± 1	726 ± 38	6.22 ± 0.39	43.4
LYS 6	sandy residuum	320	270-340	71.0	0.7528	24.59 ± 0.87	644 ± 33	5.72 ± 0.36	31.4
LYS 8 [4]	weathered rock	440 [5]	-	60.0	0.7762	16.69 ± 0.62	509 ± 26	4.90 ± 0.31	18.0
								summed inventory to depth of 4.4 m =	356.0

[1] Sampled from the middle part of each drilling case.

[2] "Reac" is sum of am-ox and x-ox fractions that were extracted separately and then combined for AMS measurement; combined analytical and blank uncertainty (all uncertainties 1σ) given.

[3] Calculated using eq. 4 in Willenbring and von Blanckenburg (2010), the given depth interval (cm), a $[^{10}Be]_{bulk}$ of $58.2x10^6$ ats g^{-1} for the (unquantified) upper 30 cm and a density of 1.5 g cm^{-3}. For the regolith core section (30-340 cm), we used a sediment density of 1.8 g cm^{-3} and the given $[^{10}Be]_{reac}$.

[4] Sample was ground prior to the sequential chemical leach.

[5] Rock fragment from the given depth.

Table 5: $[^9Be]_{parent}$ of the different bedrock types prevailing in the catchments.

Bedrock type	Average [Be] [1] (µg g^{-1})	Median [Be] (µg g^{-1})	Minimum [Be] [2] (µg g^{-1})	Maximum [Be] [2] (µg g^{-1})	n [3]
Lysina (Felsic- Granite)					
Granite	5.4 ± 4.8	3.5	2.83 ± 0.14	20.3 ± 1	14
Catchment-wide estimate [4, 5]	5.5				
Na Zeleném (Mafic- Amphibolite)					
Individual rock types:					
Amphibolite	0.69 ± 0.23	0.63	0.426 ± 0.021	1.174 ± 0.059	9
Metadolerite/-basite	2.43 ± 0.27	2.47	2.08 ± 0.10	2.89 ± 0.14	5
Average of all bedrock samples	1.32 ± 0.91	0.87	0.426 ± 0.021	2.89 ± 0.14	14
Catchment-wide estimate [4, 5]	1.21				
Pluhúv Bor (Ultramafic- Serpentinite)					
Individual rock types:					
Serpentinite	< 0.01 [6]				6
Amphibolite	0.495 ± 0.042	0.452	0.368 ± 0.018	0.727 ± 0.036	5
Ultra-/Metabasite	0.163 ± 0.064	0.225	0.102 ± 0.005	0.249 ± 0.012	3
Schist	0.249				1
Average of all bedrock samples	0.205 ± 0.238	0.102	< 0.01 [7]	0.727 ± 0.036	15
Average weighed by area [6]	0.15				
Catchment-wide estimate [4, 5]	0.18				

[1] Average value ±1SD (natural range).

[2] Value given with 5% uncertainty of ICP-OES measurement.

[3] Number of measured bedrock samples.

[4] Catchment-wide Be concentrations derived from [^{9}Be] measured in fine-grained bedload sediment (LYS) or from linear regression approach (NAZ and PLB; see Section 8.1). Value is given without uncertainty as the total uncertainty on this bedrock beryllium concentration value cannot be assessed reliably.

[5] This catchment-wide estimate is used for further calculations of the denudation rate (see Table 12).

[6] Percentage areal distribution of bedrock types from Krám et al. (2009).

[7] The detection limit of measurements is 10 ng g^{-1} of Be in the bedrock.

Table 6: Discharge, pH values, ^{10}Be and ^{9}Be concentrations, and calculated dissolved ratios for a 2-year time series of stream water samples and one groundwater sample.

Catchment	Sample type	Sampling date/ Period [1]	Discharge (L s^{-1})	pH	^{10}Be (×10^4 ats g^{-1})	^{9}Be (ng L^{-1})	^{10}Be/^{9}Be (×10^{-10})
Lysina	range [2]	3.8.11-5.2.13	0.19-13.5	4.6	11.8 ± 1.7	969 ± 82	18.4 ± 3
(felsic)	"flood"	02.06.13	112	4.0	-	574 ± 45	-
	groundwater	03.08.11	-	-	13.36 ± 0.40	2075 ± 161	9.64 ± 0.8
Na Zeleném	range [2]	3.8.11-5.2.13	0.1-26.6 [3]	7.2	1.02 ± 0.75	25 ± 14	57 ± 11
(mafic)	"flood"	02.06.13	153	6.2	-	78.8 ± 6.1	-
Pluhúv Bor	range [2]	3.8.11-6.2.13	0.1-7.0	7.8	2.1 ± 1.8	17 ± 11	168 ± 50
(ultramafic)	"flood"	02.06.13	69	6.9	-	71.9 ± 5.6	-

[1] day/month/year. On the 3.08.2011, we also sampled bedload (see Table 3) that we compare to dissolved ^{10}Be/^{9}Be data in Fig 6.

[2] Range of 10 samples (see Table S5) taken over a 2-year period given with SD of Be concentrations. Given SD is larger than uncertainty of analytical uncertainties of individual samples (mean discharge given in Table 1).

[3] Value includes four dates where discharge can only be estimated due to damaged v-notch weir. Estimated discharge on these dates is 0.1 L s^{-1}.

Table 7: *In situ*-cosmogenic ^{10}Be concentrations and calculated denudation rates from bedload sediments. LYS = Lysina (felsic), NAZ = Na Zeleném (mafic), PLB = Pluhův Bor (ultramafic).

Sample ID	Grain size (µm)	^{10}Be concentration ($x10^4$ ats g^{-1})	Total production rate [1] (ats g^{-1} y^{-1})	Denudation rate (t km^{-2} y^{-1})	Denudation rate [2] (mm ky^{-1})	Integration time scale (ky)
LYS-1	250-500	17.6 ± 1.4	8.36	101 ± 9.9	38.9 ± 3.8	15.4
LYS-2	500-800	17.69 ± 0.94	8.36	100.8 ± 8.9	38.7 ± 3.4	14.5
NAZ	125-800	17.9 ± 1.5	7.5	91.1 ± 9.9	*35.1 ± 3.8*	17.0
PLB	125-800	33.8 ± 2.6	7.57	45.6 ± 4.9	*17.5 ± 1.9*	34.2

[1] Total (muonic + spallogenic) *in situ* ^{10}Be production rate scaled after Dunai (2000) and using a spallogenic SLHL production rate of 3.7 ats g^{-1} y^{-1} (Borchers et al., 2016). We used a total production rate of 3.75 that includes the muonic production rates of Braucher et al. (2011).

[2] For conversion of units (t km^{-2} y^{-1} to mm ky^{-1}), we used a density of 2.6 g cm^{-3}, but note that this density is most likely too low for mafic and ultramafic rocks (italic values).

Table 8: K_d values for ^{10}Be and ^{9}Be (in L kg^{-1})

Catchment	pH value	K_d value (^{10}Be) - measured [1]- (L kg^{-1})	K_d value (^{9}Be) - measured [1]- (L kg^{-1})	K_d value - estimated [2]- (L kg^{-1})
Lysina (felsic)	4.2	$1.3x\ 10^3$ ± $7.0x\ 10^1$	1.2×10^3 ± 1.1×10^2	$2.1x\ 10^3$
	5.5 [3]	-	-	$1.4x\ 10^4$
Na Zeleném (mafic)	6.9	$6.1x\ 10^4$ ± $5.1x\ 10^3$	9.2×10^4 ± 8.5×10^3	$1.2x\ 10^5$
Pluhův Bor (ultramafic)	7.6	$2.7x\ 10^4$ ± $1.4x\ 10^3$	3.0×10^4 ± 2.8×10^3	$3.4x\ 10^5$

[2] K_d value calculated using (amorphous oxide-bound Be/g sediment)/(dissolved Be/mL water). We use $[Be]_{am\text{-}ox}$ for calculation (and not reactive concentrations) because as shown in section 6.2, the dissolved phase is most likely exchanging with the amorphous oxide phase in the studied catchments.

[3] K_d value estimated using y = 0.65 x pH + 0.59 derived from the linear part (pH range 0-8) of You et al.´s (1989) dataset (for details of the pH-K_d relation, see supplement of Wittmann et al., 2015).

[4] Simulated long-term (pre-industrial, i.e. prior to acid rain deposition) pH value from Hruška and Krám (2003).

Table 9: ^{10}Be flux balance

Catchment/ Grain size [1,2]	J^{10Be}_{atm} [3] (10^{15} ats y^{-1})	J^{10Be}_{diss} [4] (10^{15} ats y^{-1})	J^{10Be}_{reac} [4] (10^{15} ats y^{-1})	J^{10Be}_{riv} [4] (10^{15} ats y^{-1})	$J^{10Be}_{riv}/J^{10Be}_{atm}$ [4]
LYS "bulk"	3.938 ± 0.045	11.05 ± 1.59	0.80 ± 0.18	11.85 ± 1.60	3.01 ± 0.41
LYS "(K_d)" [5]	3.938 ± 0.045	1.55 ± 0.22	0.80 ± 0.18	2.35 ± 0.29	0.596 ± 0.073
NAZ "bulk"	8.021 ± 0.092	1.76 ± 1.29	6.9 ± 1.6	8.67 ± 2.05	1.08 ± 0.26
PLB "bulk"	3.209 ± 0.037	0.74 ± 0.62	1.13 ± 0.27	1.87 ± 0.67	0.58 ± 0.32

[1] All J^{10Be}_{reac} and J^{10Be}_{riv} calculated using $[^{10}Be]_{reac}$ data of the estimated "bulk" fraction (details Table 3), respectively. Values for the <63 µm fraction are given in supplementary Table S6. LYS = Lysina (felsic), NAZ = Na Zeleném (mafic), PLB = Pluhův Bor (ultramafic).

[2] All J^{10Be}_{diss} calculated using $[^{10}Be]_{diss}$ data from Table 6 and mean discharge and drainage area from Table 1.

[3] Atmospheric depositional ^{10}Be flux over the surface area of each catchment calculated using eq. 4 and a F^{10Be}_{met} of $1.46x10^6$ ats cm^{-2} y^{-1} for all catchments including a 10% uncertainty that is assessed from the flux provided by the adjacent cells in the depositional flux map in Heikkilä and von Blanckenburg (2015).

[4] Dissolved and particulate fluxes calculated using eq. 5. The reactive ^{10}Be flux contained on sediment was calculated using a sediment load estimated from the *in situ* ^{10}Be denudation rate and a CDF of 0.5 to subtract the weathering flux that is included in D_{insitu}.

[5] Estimate using a pre-industrial K_d value of $1.5x10^4$ (Table 8, section 6.1) representing a long-term pH value of 5.5 in Lysina, to correct for the loss of ^{10}Be to the dissolved phase, resulting in much lower J^{10Be}_{diss}.

Table 10: Compilation of beryllium concentrations measured in mafic and ultramafic rock types and serpentinite minerals

Bedrock type / Mineral Specification	Locality	^{9}Be concentration (µg g^{-1})	Reference
Amphibolite	Catalina Schist, California	0.41 - 1.10	Bebout et al. (1993)
Greenschist-amphibolite facies	Ural Mountains	0.5 - 8.0	Grew (2002)
Metabasite	Swiss-Italian Alps	0.79 - 0.86	Pelletier et al. (2008)
Serpentinite (whole rock)	Swiss-Italian Alps	0.01 - 0.04	Pelletier et al. (2008)
Serpentine minerals (serpentinized peridotites)		0.00013 - 0.016	Vils et al. (2008)

Table 11: Degree of ^{9}Be that is released by weathering

ID	$(f(^{9}Be)_{reac} + f(^{9}Be)_{diss})_{min/reac}$ "bulk" estimate
LYS (felsic)	0.100 ± 0.0052
NAZ (mafic)	0.505 ± 0.026
PLB (ultramafic)	0.371 ± 0.019

Calculated with eq. 3. Uncertainty includes uncertainties from ICP-OES measurements. Values for the <63 µm grain size fraction are given in supplementary Table S8.

Table 12: Erosion and denudation rates for the "bulk" grain size fraction

Parameters used for calculation :	**Lysina (felsic)**	**Na Zeleném (mafic)**	**Pluhův Bor (ultramafic)**
$[^{10}Be]_{reac}$ "bulk" bedload (10^{6} ats g^{-1})	58.7 ± 2.4	276 ± 10	225 ± 10
$(^{10}Be/^{9}Be)_{reac}$ "bulk" bedload (×10^{-10})	19.6 ± 1.4	31.3 ± 2	214 ± 15
$[^{9}Be]_{parent}$ (10^{16} ats g^{-1}) [1]	36.7	8.1	1.2
$[^{9}Be]_{min}$ (10^{16} ats g^{-1})	27.0 ± 1.4	8.71 ± 0.45	1.786 ± 0.093
$[^{9}Be]_{reac}$ "bulk" bedload (10^{16} ats g^{-1})	2.988 ± 0.067	8.83 ± 0.19	1.052 ± 0.029
Erosion rates (t km^{-2} y^{-1}) [2]			
without correction [4]	248 ± 27	52.8 ± 5.6	64.8 ± 7.1
measured K_d [5]	-	48.3 ± 5.1	59.8 ± 6.5
K_d from linear trendline [6]	225 ± 24	50.2 ± 5.3	64.4 ± 7.0
Denudation rates (t km^{-2} y^{-1}) [3]			
without correction [4]	203 ± 25	114 ± 15	154 ± 20
measured K_d [5]	-	110 ± 13	146 ± 19
K_d from linear trendline [6]	185 ± 23	112 ± 14	153 ± 19

For all calculations and all catchments, a depositional flux of 1.46(± 0.15)×10^{6} at cm^{-2} y^{-1} was used. In supplementary Table S9, we calculate all E and D using values of the <63 µm grain size fraction.

[1] An uncertainty on $[^{9}Be]_{parent}$ (equals 5.5 ppm for LYS, 1.2 ppm for NAZ, and 0.18 ppm for PLB) was not propagated as it cannot be assessed reliably.

[2] Calculated using eq. 1; uncertainties include 10% uncertainty on the depositional ^{10}Be flux and the analytical AMS uncertainty on the ^{10}Be concentrations.

[3] Calculated using eq. 2; uncertainties include 10% uncertainty on the depositional ^{10}Be flux and the analytical AMS and OES uncertainties on ^{10}Be and ^{9}Be concentrations, respectively.

[4] Calculated using the simplified eq. 1b (erosion rates) or eq. 2b (denudation rates) (ignoring the retentivity correction term).

[5] Calculated using eq. 1a (erosion rates) or eq. 2a (denudation rates) with a measured K_d value ((amorphous oxide-bound Be/g sediment)/(dissolved Be/ml water)).

[6] Calculated using eq. 1a (erosion rates) or eq. 2a (denudation rates) with an empirical K_d (Table 8). For Lysina the K_d value equal to a modeled pre-industrial pH of 5.5. was used (Table 8).

References

Barg, E., Lal, D., Pavich, M.J., Caffee, M.W. and Southon, J.R. (1997) Beryllium geochemistry in soils: evaluation of Be-10/Be-9 ratios in authigenic minerals as a basis for age models. Chemical Geology 140, 237-258.

Bebout, G.E., Ryan, J. G., Lemman, W.P. (1993) B-Be systematics in subduction-related metamorphic rocks: Characterization of the subducted component. GCA, 57, 2227-2237.

Belmont, P., Willenbring, J.K., Schottler, S.P., Marquard, J., Kumarasamy, K. and Hemmis, J.M. (2014) Toward generalizable sediment fingerprinting with tracers that are conservative and nonconservative over sediment routing timescales. Journal of Soils and Sediments 14, 1479-1492.

Berner, R.A. (1995) Chemical weathering and its effect on atmospheric CO_2 and climate. Reviews in Mineralogy and Geochemistry 31, 565-583.

Bierman, P.R. and Nichols, K.K. (2004) Rock to sediment - Slope to sea with Be-10 - Rates of landscape change. Annual Review of Earth and Planetary Sciences 32, 215-255.

Blecha, V. and Štemprok, M. (2012) Petrophysical and geochemical characteristics of late Variscan granites in the Karlovy Vary Massif (Czech Republic) - implications for gravity and magnetic interpretation in shallow depths. Journal of Geosciences 57, 65-85.

Bouchez, J., Gaillardet, J., France-Lanord, C., Maurice, L. and Dutra-Maia, P. (2011) Grain size control of river suspended sediment geochemistry: Clues from Amazon River depth profiles. Geochemistry Geophysics Geosystems 12, Q03008.

Brown, E.T., Edmond, J.M., Raisbeck, G.M., Bourles, D.L., Yiou, F. and Measures, C.I. (1992) Beryllium Isotope Geochemistry in Tropical River Basins. Geochimica Et Cosmochimica Acta 56, 1607-1624.

Brown, L., Pavich, M.J., Hickman, R.E., Klein, J. and Middleton, R. (1988) Erosion of the eastern United States observed with ^{10}Be. Earth Surface Processes and Landforms 13, 441-457.

Chmeleff, J., von Blanckenburg, F., Kossert, K. and Jakob, D. (2010) Determination of the ^{10}Be half-life by multicollector ICP-MS and liquid scintillation counting. Nuclear Instruments & Methods in Physics Research Section B- Beam Interactions with Materials and Atoms 268, 192-199.

Christl, M., Vockenhuber, C., Kubik, P.W., Wacker, L., Lachner, J., Alfimov, V. and Synal, H.A. (2013) The ETH Zurich AMS facilities: Performance parameters and reference materials. Nuclear Instruments and Methods in Physics Research Section B: Beam Interactions with Materials and Atoms 294, 29-38.

Cleaves, E.T., Fisher, D.W. and Bricker, O.P. (1974) Chemical weathering of serpentinite in the eastern Piedmont of Maryland. Geological Society of America Bulletin 85, 437-444.

Codilean, A.T., Fenton, C.R., Fabel, D., Bishop, P. and Xu, S. (2014) Discordance between cosmogenic nuclide concentrations in amalgamated sands and individual fluvial pebbles in an arid zone catchment. Quaternary Geochronology 19, 173-180.

Cudennec, Y. and Lecerf, A. (2006) The transformation of ferrihydrite into goethite or hematite, revisited. Journal of Solid State Chemistry 179, 716-722.

Czudek, T. (1993) Pleistocene periglacial structures and landforms in Western Czechoslovakia. Permafrost and Periglacial Processes 4, 65-75.

Dessert, C., Dupré, B., Gaillardet, J., François, L.M. and Allègre, C.J. (2003) Basalt weathering laws and the impact of basalt weathering on the global carbon cycle. Chemical Geology 202, 257-273.

Dewald, A., Heinze, S., Jolie, J., Zilges, A., Dunai, T., Rethemeyer, J., Melles, M., Staubwasser, M., Kuczewski, B., Richter, J., Radtke, U., von Blanckenburg, F. and Klein, M. (2013) CologneAMS, a dedicated center for accelerator mass spectrometry in Germany. Nuclear Instruments and Methods in Physics Research Section B: Beam Interactions with Materials and Atoms 294, 18-23.

Dixon, J.L. and von Blanckenburg, F. (2012) Soils as pacemakers and limiters of global silicate weathering. Comptes Rendus Geoscience 344, 597-609.

Drever, J.I. (1997) The geochemistry of natural waters: surface and groundwater environments. Englewood Cliffs, N.J., Prentice-Hall

Ebert, K., Willenbring, J., Norton, K.P., Hall, A. and Hättestrand, C. (2012) Meteoric ^{10}Be concentrations from saprolite and till in northern Sweden: Implications for glacial erosion and age. Quaternary Geochronology 12, 11-22.

Egli, M., Brandová, D., Böhlert, R., Favilli, F. and Kubik, P.W. (2010) ^{10}Be inventories in Alpine soils and their potential for dating land surfaces. Geomorphology 119, 62-73.

Frank, M., Porcelli, D., Andersson, P., Baskaran, M., Bjork, G., Kubik, P.W., Hattendorf, B. and Guenther, D. (2009) The dissolved Beryllium isotope composition of the Arctic Ocean. Geochimica Et Cosmochimica Acta 73, 6114-6133.

Gaillardet, J., Dupré, B., Louvat, P. and Allègre, C.J. (1999) Global silicate weathering and CO_2 consumption rates deduced from the chemistry of large rivers. Chemical Geology 159, 3-30.

Gaillardet, J., Louvat, P. and Lajeunesse, E. (2011) Rivers from Volcanic Island Arcs: The subduction weathering factory. Applied Geochemistry 26, Supplement, S350-S353.

Gayer, E., Mukhopadhyay, S. and Meade, B.J. (2008) Spatial variability of erosion rates inferred from the frequency distribution of cosmogenic ^{3}He in olivines from Hawaiian river sediments. Earth and Planetary Science Letters 266, 303-315.

Grew, E.S. (2002) Beryllium in metamorphic environments (emphasis on aluminous compositions). Reviews in Mineralogy and Geochemistry, 50, 487-549.

Goodwin, P., Williams, R.G., Ridgwell, A. and Follows, M.J. (2009) Climate sensitivity to the carbon cycle modulated by past and future changes in ocean chemistry. Nature Geoscience 2, 145-150.

Goudie, A.S. and Viles, H.A. (2012) Weathering and the global carbon cycle: Geomorphological perspectives. Earth-Science Reviews 113, 59-71.

Graly, J.A., Bierman, P.R., Reusser, L.J. and Pavich, M.J. (2010) Meteoric ^{10}Be in soil profiles - A global meta-analysis. Geochimica et Cosmochimica Acta 74, 6814-6829.

Graly, J.A., Reusser, L.J. and Bierman, P.R. (2011) Short and long-term delivery rates of meteoric ^{10}Be to terrestrial soils. Earth and Planetary Science Letters 302, 329-336.

Granger, D.E. and Schaller, M. (2014) Cosmogenic Nuclides and Erosion at the Watershed Scale. Elements 10, 369-373.

Heikkilä, U., Beer, J., Abreu, J.A. and Steinhilber, F. (2013a) On the Atmospheric Transport and Deposition of the Cosmogenic Radionuclides (10Be): A Review. Space Science Reviews 176, 321-332.

Heikkilä, U., Phipps, S.J. and Smith, A.M. (2013b) Be-10 in late deglacial climate simulated by ECHAM5-HAM - Part 1: Climatological influences on Be-10 deposition. Climate of the Past 9, 2641-2649.

Heikkilä, U. and von Blanckenburg, F. (2015) The global distribution of Holocene meteoric ^{10}Be fluxes from atmospheric models. Distribution maps for terrestrial Earths surface applications. GFZ Data Services, GFZ Potsdam.

Hruška, J. and Krám, P. (2003) Modelling long-term changes in stream water and soil chemistry in catchments with contrasting vulnerability to acidification (Lysina and Pluhuv Bor, Czech Republic). Hydrology and Earth System Sciences 7, 525-539.

Ibarra, D.E., Caves, J.K., Moon, S., Thomas, D.L., Hartmann, J., Chamberlain, C.P. and Maher, K. (2016) Differential weathering of basaltic and granitic catchments from concentration–discharge relationships. Geochimica et Cosmochimica Acta 190, 265-293.

Jeandel, C. (1993) Concentration and isotopic composition of Nd in the South Atlantic Ocean. Earth and Planetary Science Letters 117, 581-591.

Jelínek, E. and Štědrá, V. (1997) Petrology and geochemistry of the Mariánské Lázně Complex, in: Vrána, S., Štědrá, V. (Eds.), Geological model of Western Bohemia related to the KTB borehole in Germany. Czech Geological Survey, Prague, pp. 63-65.

Jelínek, E., Štedrá, V. and Cháb, J. (1997) The Mariánské Lázne complex, in: Vrána, S., Štědrá, V. (Eds.), Geological model of western Bohemia related to the KTB borehole in Germany. Czech Geological Survey, Prague, p. 61.

Jungers, M.C., Bierman, P.R., Matmon, A., Nichols, K., Larsen, J. and Finkel, R. (2009) Tracing hillslope sediment production and transport with in situ and meteoric10Be. Journal of Geophysical Research 114.

Korschinek, G., Bergmaier, A., Faestermann, T., Gerstmann, U.C., Knie, K., Rugel, G., Wallner, A., Dillmann, I., Dollinger, G., von Gostomski, C.L., Kossert, K., Maiti, M., Poutivtsev, M. and Remmert, A. (2010) A new value for the half-life of ^{10}Be by heavy-ion elastic recoil detection and liquid scintillation counting. Nuclear Instruments & Methods in Physics Research Section B- Beam Interactions with Materials and Atoms 268, 187-191.

Krám, P. and Hruška, J. (1994) Influence of bedrock geology on elemental fluxes in two forested catchments affected by high acidic deposition. Hydrogeology Journal 2, 50-58.

Krám, P., Hruška, J. and Shanley, J.B. (2012) Streamwater chemistry in three contrasting monolithologic Czech catchments. Applied Geochemistry 27, 1854-1863.

Krám, P., Myška, O., Čuřík, J., Veselovský, F. and Hruška, J. (2013) Drainage water chemistry in geochemically contrasting catchments, in: R. Stojanov, Z.Ž., P. Cudlín, A. Farda, O. Urban, M. Trnka (Ed.), Global change and resilience, from impacts to responses, Global Change Research Centre AS CR. Brno, pp. 173-177.

Krám, P., Oulehle, F., Štědrá, V., Hruška, J., Shanley, J.B., Minocha, R. and Traister, E. (2009) Geoecology of a forest watershed underlain by serpentine in Central Europe. Northeastern Naturalist 16, 309-328.

Lal, D. (1991) Cosmic ray labeling of erosion surfaces: in situ nuclide production rates and erosion models. Earth and Planetary Science Letters 104, 424-439.

Ludwig, W., Probst, J.-L. and Kempe, S. (1996) Predicting the oceanic input of organic carbon by continental erosion. Global Biogeochemical Cycles 10, 23-41.

Maher, K. and von Blanckenburg, F. (2016) Surface ages and weathering rates from ^{10}Be(meteoric) and ^{10}Be/^{9}Be: insights from differential mass balance and reactive transport modeling. Chemical Geology 446, 70-86.

Masarik, J. and Beer, J. (1999) Simulation of particle fluxes and cosmogenic nuclide production in the Earth's atmosphere. Journal of Geophysical Research: Atmospheres 104, 12099-12111.

Mckean, J.A., Dietrich, W.E., Finkel, R.C., Southon, J.R. and Caffee, M.W. (1993) Quantification of Soil Production and Downslope Creep Rates from Cosmogenic Be-10 Accumulations on a Hillslope Profile. Geology 21, 343-346.

Menon, M., Rousseva, S., Nikolaidis, N., van Gaans, P., Panagos, P., de Souza, D., Ragnarsdottir, K., Lair, G., Weng, L., Bloem, J., Kram, P., Novak, M., Davidsdottir, B., Gisladottir, G., Robinson, D., Reynolds, B., White, T., Lundin, L., Zhang, B., Duffy, C., Bernasconi, S., de Ruiter, P., Blum, W.H. and Banwart, S. (2014) SoilTrEC: a global initiative on critical zone research and integration. Environ Sci Pollut Res 21, 3191-3195.

Meybeck, M. (1987) Global chemical weathering of surficial rocks estimated from river dissolved loads. American Journal of Science 287, 401-428.

Meyer, H., Hetzel, R. and Strauss, H. (2010) Erosion rates on different timescales derived from cosmogenic ^{10}Be and river loads: implications for landscape evolution in the Rhenish Massif, Germany. International Journal of Earth Sciences 99, 395-412.

Milliman, J.D. and Farnsworth, K.L. (2011) River Discharge to the Coastal Ocean: A Global Synthesis. Cambridge University Press, U.K., Cambridge.

Milliman, J.D. and Syvitski, J.P.M. (1992) Geomorphic tectonic control of sediment discharge to the ocean- The importance of small mountainous rivers. Journal of Geology 100, 525-544.

Navrátil, T. (2000) Beryllium in waters of Czech forested ecosystems and the release of beryllium from granites. GeoLines 12, 18-40.

Navrátil, T., Skřivan, P., Minařík, L. and Žigová, A. (2002) Beryllium geochemistry in the Lesni potok catchment (Czech Republic), 7 years of systematic study. Aquatic Geochemistry 8, 121-134.

Neilson, T.B., Schmidt, A.H., Bierman, P.R., Rood, D.H. and Sosa Gonzalez, V. (2017) Efficacy of in situ and meteoric 10 Be mixing in fluvial sediment collected from small catchments in China. Chemical Geology 471, 119-130.

Oliva, P., Viers, J. and Dupré, B. (2003) Chemical weathering in granitic environments. Chemical Geology 202, 225-256.

Ouimet, W., Dethier, D., Bierman, P., Wyshnytzky, C., Shea, N. and Rood, D.H. (2015) Spatial and temporal variations in meteoric ^{10}Be inventories and long-term deposition rates, Colorado Front Range. Quaternary Science Reviews 109, 1-12.

Pačes, T. (1985) Sources of acidification in Central Europe estimated from elemental budgets in small basins. Nature 315, 31-36.

Pačes, T. (1986) Rates of weathering and erosion derived from mass balance in small drainage basins, in: Colman, S.M., Dethier, D.P. (Ed.), Rates of Chemical Weathering of Rocks and Minerals. Academic Press, INC. , Orlando, pp. 531-550.

Pavich, M.J., Brown, L., Harden, J., Klein, J. and Middleton, R. (1986) 10Be distribution in soils from Merced River terraces, California. Geochimica et Cosmochimica Acta 50, 1727-1735.

Pelletier, L., Müntener, O., Kalt, A., Vennemann, T.W., Belgya, T. (2008) Emplacement of ultramafic rocks into the continental crust monitored by light and other trace elements: An example from the Geisspfad body (Swiss-Italian Alps). Chem. Geol., 255, 143-159.

Peucker-Ehrenbrink, B. (2009) Land2Sea database of river drainage basin sizes, annual water discharges, and suspended sediment fluxes. Geochemistry Geophysics Geosystems 10, Q06014.

Pinet, P. and Souriau, M. (1988) Continental erosion and large-scale relief. Tectonics 7, 563-582.

Portenga, E.W., Bishop, P., Rood, D.H. and Bierman, P.R. (2017) Combining bulk sediment OSL and meteoric10Be fingerprinting techniques to identify gully initiation sites and erosion depths. Journal of Geophysical Research: Earth Surface 122, 513-527.

Puchol, N., Blard, P.H., Pik, R., Tibari, B. and Lave, J. (2017) Variability of magmatic and cosmogenic He-3 in Ethiopian river sands of detrital pyroxenes: Impact on denudation rate determinations. Chemical Geology 448, 13-25.

Raab, T., Leopold, M. and Völkel, J. (2007) Character, age, and ecological significance of Pleistocene periglacial slope deposits in Germany. Physical Geography 28, 451-473.

Rahaman, W., Wittmann, H. and von Blanckenburg, F. (2017) Denudation rates and the degree of chemical weathering in the Ganga basin from ratios of meteoric cosmogenic ^{10}Be to stable ^{9}Be Earth and Planetary Science Letters 469, 156-169.

Regelink, I.C., Stoof, C.R., Rousseva, S., Weng, L., Lair, G.J., Kram, P., Nikolaidis, N.P., Kercheva, M., Banwart, S. and Comans, R.N.J. (2015) Linkages between aggregate formation, porosity and soil chemical properties. Geoderma 247–248, 24-37.

Reuss, J.O., Cosby, B.J. and Wright, R.F. (1987) Chemical processes governing soil and water acidification. Nature 329, 27-32.

Reusser, L.J. and Bierman, P.R. (2010) Using meteoric 10Be to track fluvial sand through the Waipaoa River basin, New Zealand. Geology 38, 47-50.

Rudnick, R.L. and Gao, S. (2004) Composition of the Continental Crust, in: Heinrich, D.H., Karl, K.T. (Eds.), Treatise on Geochemistry. Elsevier, Amsterdam, pp. 1-64.

Schaller, M., von Blanckenburg, F., Hovius, N. and Kubik, P.W. (2001) Large-scale erosion rates from in situ-produced cosmogenic nuclides in European river sediments. Earth and Planetary Science Letters 188, 441-458.

Schaller, M., von Blanckenburg, F., Veit, H. and Kubik, P.W. (2002a) Influence of periglacial cover beds on in situ-produced cosmogenic 10Be in soil sections. Geomorphology 49, 255-267.

Schaller, M., von Blanckenburg, F., Veldkamp, A., Tebbens, L.A., Hovius, N. and Kubik, P.W. (2002b) A 30 000 yr record of erosion rates from cosmogenic Be-10 in Middle European river terraces. Earth and Planetary Science Letters 204, 307-320.

Schopka, H.H., Derry, L.A. and Arcilla, C.A. (2011) Chemical weathering, river geochemistry and atmospheric carbon fluxes from volcanic and ultramafic regions on Luzon Island, the Philippines. Geochimica Et Cosmochimica Acta 75, 978-1002.

Schwertmann, U., Friedl, J. and Stanjek, H. (1999) From Fe(III) Ions to Ferrihydrite and then to Hematite. Journal of Colloid and Interface Science 209, 215-223.

Shen, C., Beer, J., Kubik, P.W., Suter, M., Borkovec, M. and Liu, T.S. (2004) Grain size distribution, ^{10}Be content and magnetic susceptibility of micrometer-nanometer loess materials. Nuclear Instruments and Methods in Physics Research Section B: Beam Interactions with Materials and Atoms 223-224, 613-617.

Singleton, A.A., Schmidt, A.H., Bierman, P.R., Rood, D.H., Neilson, T.B., Greene, E.S., Bower, J.A. and Perdrial, N. (2017) Effects of grain size, mineralogy, and acid-extractable grain coatings on the distribution of the fallout radionuclides ^{7}Be, ^{10}Be, ^{137}Cs, and ^{210}Pb in river sediment. Geochimica et Cosmochimica Acta 197, 71-86.

Štědrá, V., Jarchovský, T. and Krám, P. (2016) Lithium-rich granite in the Lysina-V1 borehole in the southern part of the Slavkov Forest, western Bohemia. Geoscience Research Reports 49, 137-142.

Štědrá, V., Krám, P. and Farkaš, J. (2015) Petrology and whole-rock geochemistry of metabasites from borehole cores in the Na Zeleném and Pluhův Bor catchments in the Slavkov Forest, western Bohemia. Geoscience Research Reports for 2014 2014, 103-108.

Summerfield, M.A. and Hulton, N.J. (1994) Natural controls of fluvial denudation rates in major world drainage basin. Journal of Geophysical Research-Solid Earth 99, 13871-13883.

Valette-Silver, J.N., Brown, L., Pavich, M., Klein, J. and Middleton, R. (1986) Detection of erosion events using 10Be profiles: example of the impact of agriculture on soil erosion in the Chesapeake Bay area (U.S.A.). Earth and Planet. Sc. Letters 80, 82-90.

Vanmaercke, M., Poesen, J., Verstraeten, G., de Vente, J. and Ocakoglu, F. (2011) Sediment yield in Europe: Spatial patterns and scale dependency. Geomorphology 130, 142-161.

Vils, F., Pelletier, L., Kalt, A., Müntener, O., Ludwig, T. (2008) The Lithium, Boron, and Beryllium content of serpentinized peridotites from ODP Leg 209 (Sites 1272A and 1274A): Implications for lithium and boron budgets of oceanic lithosphere. GCA, 72, 5475-5504.

von Blanckenburg, F. (2005) The control mechanisms of erosion and weathering at basin scale from cosmogenic nuclides in river sediment. Earth and Planetary Science Letters 237, 462-479.

von Blanckenburg, F., Belshaw, N.S. and O'Nions, R.K. (1996) Separation of ^{9}Be and cosmogenic ^{10}Be from environmental materials and SIMS isotope dilution analysis. Chemical Geology 129, 93-99.

von Blanckenburg, F., Bouchez, J. and Wittmann, H. (2012) Earth surface erosion and weathering from the ^{10}Be (meteoric)/^{9}Be ratio. Earth and Planetary Science Letters 351-352, 295-305.

von Blanckenburg, F. and Willenbring, J.K. (2014) Cosmogenic nuclides: dates and rates of Earth-surface change. Elements 10, 341-346.

Waychunas, G.A., Kim, C.S. and Banfield, J.F. (2005) Nanoparticulate iron oxide minerals in soils and sediments: unique properties and contaminant scavenging mechanisms. J. Nanopart. Res. 7, 409-433.

West, N., Kirby, E., Bierman, P., Slingerland, R., Ma, L., Rood, D. and Brantley, S. (2013) Regolith production and transport at the Susquehanna Shale Hills Critical Zone Observatory, Part 2: Insights from meteoric10Be. Journal of Geophysical Research: Earth Surface 118, 1877-1896.

Willenbring, J.K. and von Blanckenburg, F. (2010) Meteoric cosmogenic Beryllium-10 adsorbed to river sediment and soil: Applications for Earth-surface dynamics. Earth-Science Reviews 98, 105-122.

Wittmann, H. and von Blanckenburg, F. (2016) The geological significance of cosmogenic nuclides in large lowland river basins. Earth Science Reviews 159, 118-141.

Wittmann, H., von Blanckenburg, F., Bouchez, J., Dannhaus, N., Naumann, R., Christl, M. and Gaillardet, J. (2012) The dependence of meteoric ^{10}Be concentrations on particle size in Amazon River bed sediment and the extraction of reactive ^{10}Be/^{9}Be ratios. Chemical Geology 318-319, 126-138.

Wittmann, H., von Blanckenburg, F., Dannhaus, N., Bouchez, J., Guyot, J.L., Maurice, L., Roig, H., Filizola, N., Gaillardet, J. and Christl, M. (2015) A test of the new cosmogenic ^{10}Be(meteoric)/^{9}Be proxy for simultaneously determing basin-wide erosion rates, denudation rates, and the degree of weathering in the Amazon basin. Journal of Geophysical Research- Earth Surface 120, 2498-2528.

You, C.-F., Lee, T. and Li, Y.-H. (1989) The partition of Be between soil and water. Chemical Geology 77, 105-118.

You, C.F., Lee, T., Brown, L., Shen, J.J. and Chen, J.C. (1988) ^{10}Be study of rapid erosion in Taiwan. Geochimica et Cosmochimica Acta 52, 2687-2691.